# Dorsal peduncular cortex activity modulates affective behaviors in mice

Justin J. Botterill[1,2*], Abdessattar Khlaifia[1*], Ryan Appings[1], Hanista Premachandran[1], Arely Cruz-Sanchez[1,3], Maithe Arruda-Carvalho[1,3†]

1. Department of Psychology, University of Toronto Scarborough, Toronto, ON, M1C1A4, Canada
2. Department of Anatomy, Physiology, and Pharmacology, University of Saskatchewan, Saskatoon, SK, S7N 5E5, Canada.
3. Department of Cell and Systems Biology, University of Toronto, Toronto, ON, M5S3G5, Canada.

**Abstract**

The medial prefrontal cortex (mPFC) is critically involved in cognitive and emotional function and underlies many neuropsychiatric disorders, including mood, fear and anxiety disorders. In rodents, disruption of mPFC activity affects anxiety- and depression-like behavior, with evidence supporting specialized contributions from its subdivisions. The rodent mPFC is often subdivided into the anterior cingular cortex (ACC), prelimbic cortex (PL), and the infralimbic cortex (IL), and broken down into the dorsomedial prefrontal cortex (dmPFC), spanning ACC and dorsal PL, and the ventromedial prefrontal cortex (vmPFC), which includes the ventral PL, IL, and in some studies the dorsal peduncular cortex (DP) and dorsal tenia tecta (DTT). The DP/DTT have recently been implicated in the regulation of stress-induced sympathetic responses via projections to the hypothalamus. While many studies implicate the PL and IL in anxiety-, depression-like and fear behavior, the contribution of the DP/DTT to affective and emotional behavior remains unknown. Here, we used chemogenetics to bidirectionally modulate DP/DTT activity and examine its effects on affective behaviors, cognition and stress responses in naïve male and female C57BL/6J mice. We found that acute chemogenetic activation of DP/DTT neurons caused a significant increase in anxiety-like behavior in the open field and elevated plus maze tests, as well as in passive coping in the tail suspension test. In contrast, chemogenetic inhibition of the DP/DTT had no effect on affective behavior, but facilitated auditory fear memory acquisition without affecting memory retrieval. Additionally, DP/DTT activation led to an increase in plasma corticosterone levels. These findings point to the DP/DTT as a new regulator of affective behavior in mice.

**Keywords:**

Prefrontal cortex, adeno-associated virus, anxiety, memory, DREADDs, electrophysiology

*JJB and AK contributed equally to this work.

†*Corresponding Author:*

Dr. Maithe Arruda-Carvalho
Department of Psychology
University of Toronto Scarborough
Toronto, Ontario, M1C1A4, Canada
Email: m.arrudacarvalho@utoronto.ca

## Introduction

The medial prefrontal cortex (mPFC) is a key brain region involved in high-order functions such as attention [1,2], decision making [3,4], working memory [5,6], social behavior [7–10], mood [11,12] and anxiety [7,13–30]. The mPFC integrates inputs from cortical sensory and motor systems, as well as subcortical brain structures [31–36] toward top-down control of output structures such as the amygdala, thalamus, hypothalamus and bed nucleus of the stria terminalis (BNST) [31,34,36–38]. Despite a lack of unified consensus [39], many studies consider the rodent mPFC to be anatomically subdivided into the anterior cingulate cortex (ACC), prelimbic cortex (PL), and the infralimbic cortex (IL) [40], with some dividing the mPFC into two main regions with differences in their connectivity pattern and functional properties [40–43]: the dorsal mPFC (dmPFC), which includes the ACC and dorsal PL, and the ventral mPFC (vmPFC), which comprises the ventral PL, IL and the dorsal peduncular cortex (DP) and dorsal tenia tecta (DTT). Altered mPFC activity underlies many neuropsychiatric disorders, including mood, fear and anxiety disorders [38,44–52]. In rodents, disruption of mPFC activity through lesions, pharmacology, optogenetics or chemogenetics affects anxiety- [21,53–55] and depression-like [56–59] behavior, with evidence supporting specialized contributions from PL and IL subdivisions [15–19,30], as well as their subprojections [58,60]. Similarly, the PL and IL mPFC subdivisions exert distinct roles in auditory fear processing [61–66]. Despite a considerable body of work implicating the mPFC as a key regulator of affective behavior and emotional learning, most studies focus on its main subdivisions, ACC, PL and IL, leaving subregions such as the DP/DTT understudied.

The DP/DTT is located at the ventral limit of the vmPFC [67], and plays a crucial role in driving thermoregulatory and cardiovascular sympathetic responses during stress [68–70]. The DP/DTT receives inputs from stress and emotion-related brain regions like the thalamus, amygdala, insular cortex and piriform cortex [68–70], and sends glutamatergic excitatory input to the dorsomedial hypothalamus (DMH), a central hub driving sympathetic responses to various stimuli, including psychosocial stress [68,70]. Interestingly, while dmPFC activation abrogates stress-related autonomic and neuroendocrine responses [71–74], DP/DTT activation mimics sympathetic responses to psychosocial stress [68], suggesting a distinct role for the DP/DTT in driving sympathetic stress responses. Given the high prevalence of sympathetic system impairments in anxiety disorders [75–78] and the well-established role of the mPFC in modulating anxiety-, depression-like and cognitive behavior in rodents, we investigated the contribution of the DP/DTT to affective behavior and emotional learning in mice. Our results show that chemogenetic activation of DP/DTT with Designer Receptors Exclusively Activated by Designer Drugs (DREADDs) in C57BL/6J mice increases anxiety-like behaviors in the open field (OFT) and elevated plus maze (EPM) tests, as well as passive coping in the tail suspension test (TST). The anxiogenic effect of DP/DTT activation was accompanied by an increase in plasma corticosterone levels. Chemogenetic inhibition of DP/DTT neurons did not significantly affect anxiety- or depression-like behaviors in mice, but slightly potentiated auditory fear acquisition without affecting fear memory retrieval. These findings uncover a novel role for the DP/DTT in promoting anxiety-like behaviors in mice.

## Materials and Methods

### Animals

Adult male and female C57BL/6J mice (2-4 months old) were used for all experiments. Mice were maintained on a 12 hr light-dark cycle (lights on at 7:00 A.M.) and all experimental procedures were done during the light phase of the light-dark cycle. Mice were bred in-house and weaned on postnatal day 21 with same-sex siblings (2-4 per cage) in standard laboratory

rodent cages that contained corn cob bedding and a polycarbonate igloo shelter (Bio-Serv). Food and water were available *ad libitum* throughout the duration of the experiment. All experimental procedures were approved by the Animal Care Committee at the University of Toronto. Experimenters were blinded for all quantitative analyses.

**Stereotaxic surgery and viral injections**

Mice between 8-12 weeks of age underwent stereotaxic surgery using procedures described previously [79,80]. Mice were injected with a cocktail of ketamine (100mg/kg) and xylazine (5mg/kg) to induce anesthesia. Once mice were fully anesthetized, the head was shaved and swabbed with iodine followed by 70% ethanol. Tear gel (Alcon) was applied to each eye to prevent dehydration. Mice were then secured in a rodent stereotaxic apparatus (Stoelting) using ear bars. Body temperature was maintained at 37°C throughout surgery with a far infrared homeothermic warming pad with a temperature feedback module (RightTemp® Jr, Kent Scientific). A scalpel was used to make an incision down the midline of the scalp, the connective tissue was excised, and the skull was cleaned with sterile phosphate buffered saline (PBS, pH=7.4). An autoclaved cotton tip applicator was briefly submerged in 30% hydrogen peroxide and then gently applied to the skull to identify bregma. A cordless micro drill (#58610, Stoelting) was used to make craniotomies over the DP (+1.85 anterior-posterior, ±0.38 medial-lateral, in reference to bregma). Virus was delivered with a 500nL Neuros Syringe (#65457-02, Hamilton Company) attached to a probe holder on the stereotaxic apparatus (#751873, Harvard Apparatus). For each injection, the syringe was positioned above each craniotomy and the needle was lowered 3.52mm below the skull surface. A total of 40nL of virus was injected at a rate of 20nL per minute. The needle stayed in place for 5 minutes after each injection to allow for diffusion of the virus before being slowly removed from the brain. We used the following adeno-associated viruses (AAVs): AAV5-hSyn-mCherry (2.3 x $10^{13}$ vg/mL, Addgene #114472), AAV5-hSyn-hM4D(Gi)-mCherry (8.6 x $10^{12}$ vg/mL, Addgene #50475), and AAV5-hSyn-hM3D(Gq)-mCherry (1.9 x $10^{13}$ vg/mL, Addgene #50474). Ketoprofen (1 mg/kg, s.c.) was used to reduce discomfort. Upon completing the viral injections, the skull was cleaned with sterile PBS and the scalp was sutured with Vetbond tissue adhesive (3M). Warmed physiological saline (0.5 to 0.7mL, s.c.) was injected at the end of each surgery to support hydration. Mice were placed in a clean cage located on a heating pad for post-surgical recovery and returned to the colony room once fully ambulatory. Ketoprofen (1 mg/kg, s.c.) was injected 24 and 48hr intervals after surgery to reduce post-surgical discomfort.

**Behavioral testing**

Mice received a 2-week postsurgical recovery period prior to behavioral testing. A total of 5 behavioral tests were used and occurred in the same order for each cohort of mice: 1) open field test (OFT), 2) elevated plus maze (EPM), 3) tail suspension test (TST), 4) forced swim test (FST) and 5) auditory fear conditioning. Prior to the start of each test, mice were moved to a dedicated room and weighed. The DREADD agonist C21 (2mg/kg, 0.5mg/mL, i.p.) was injected 1hr before the start of each behavioral test via a 0.3mL insulin syringe. Mice remained in their homecage until behavioral testing began. Methods for each behavioral test are described below. Upon completing behavioral testing, mice were returned to their homecage and left undisturbed until the next test. A 3-day washout period was used between subsequent behavioral tests. All behavioral testing apparatuses were cleaned with 70% ethanol followed by $ddH_20$ between subjects.

**Open Field Test**

Exploratory and anxiety-like behaviors were measured in the OFT as previously described [80–83] with minor modifications. Mice were placed in the corner of a brightly illuminated open field

arena (30cm length x 30cm width x 30cm height) and an overhead monochrome video camera (DMK 22AUC03, The Imaging Source) recorded behavior over the 8-minute test duration with ANY-maze software (version 7.1, Stoelting). The primary measures of interest included the time spent in the center zone of the maze (10cm x 10cm), time spent in the outer zone, and the total distance travelled during the test. Track plots and heat maps were generated using ANY-maze software.

**Elevated Plus Maze**

Exploratory and anxiety-like behaviors were evaluated in the EPM as previously described [83,84] with minor modifications. The EPM apparatus was comprised of two open and two closed arms of identical dimensions (35cm length x 10cm width) raised 51.5cm above the floor. The closed arms had 30cm tall walls, whereas the open arms had a 0.1cm raised ledge to prevent mice from falling off the apparatus during testing. At the start of each test, mice were placed in the middle of the platform (10cm length x 10cm width) with their head facing towards one of the closed arms. A Logitech C920 1080P webcam was placed directly above the EPM and recorded behavior over the 5-minute test duration via Logi Capture Software (v 2.06.12, Logitech). Video recordings were loaded in ANY-maze software and EPM behavior was analyzed offline. The primary measures of interest included the time mice spent in the open and closed arms of the EPM and the time spent in the middle platform. The software also tracked the number of entries into each zone and the total distance travelled during the test. Track plots and heatmaps were generated using ANY-maze software.

**Tail Suspension Test**

The tail suspension test (TST) was used to measure passive coping behavior as previously described [85,86]. Mice were suspended approximately 45 cm above the floor by their tails for 6 minutes. Laboratory tape was placed <1cm from the tip of each tail and secured to a horizontal stainless-steel rod attached to a laboratory retort stand. Pairs of mice were positioned approximately 40cm apart from each other during testing. A Logitech C920 1080P webcam was placed horizontally in front of the mice and recorded behavior over the test duration. The final 4 minutes of the TST was analyzed using the open-source software Depression Behavior Scorer (DBscorer), which performs automated and unbiased behavioral scoring [87]. This software converts each video frame to a binary image and compares the percent area difference between each frame, which are averaged for every second of the test duration. When the percent area difference is below a user-defined threshold value, the animal is considered immobile. Pilot experiments found that a 0.6% area threshold value was consistent with manually scored videos. The data was automatically scored in 60s time bins and consists of the percent time spent immobile, the longest continuous bout of immobility during the test (in seconds), and the number of mobility-immobility transitions. The software also automatically generated raster plots of immobility over the test duration for each mouse.

**Forced Swim Test**

The forced swim test (FST) was used to measure depression-like behavior [88–90]. Mice were individually placed in a 1L beaker (14.5cm tall) that was filled with approximately 750mL of warmed tap water (25°C). A Logitech C920 1080P webcam was placed horizontally in front of the beaker and recorded behavior for 6 minutes. The final 4 minutes of the FST was analyzed [91,92] using DBscorer with an area threshold value of 1.0% [87]. Videos were scored in 60s time bins and measured the percent of time spent immobile, the longest continuous bout of immobility (in seconds), and the number of mobility-immobility transitions. Raster plots were also generated to indicate periods of mobility and immobility throughout the 4-minute analysis period. Upon completing the FST, mice were dried off with a towel, placed in a fresh cage on a

heating blanket for 30 minutes, and returned to the colony room. The water in each beaker was changed between subjects.

**Auditory Fear Conditioning**

Auditory fear conditioning was used to evaluate whether manipulations of the DP/DTT influenced cognition. Auditory fear training occurred in a stainless-steel fear conditioning apparatus (32cm wide, 25.5cm high, 25.5cm deep) that contained shock-grid floors (36 rods, 2mm diameter; Context A). The fear conditioning apparatus was located within a sound-attenuated chamber (63.5cm wide, 36.8cm, high, 74.9cm deep; catalog #NIR-022MD, Med Associates). On the training day, a two-minute acclimation period was provided to assess baseline freezing behavior. A total of 6 auditory tones (2 kHz, 80 dB, 25s) were presented with a 60s interval and co-terminated with a 2s foot shock (0.5mA), adapted from our previous studies [64,93]. Upon completing the training session, mice were placed in their home cage and returned to the colony room until the following day.

Fear memory was evaluated 24 hours after the training session. The fear conditioning apparatus was modified for memory retrieval by installing a curved white plastic insert along the walls and a white plastic insert over the shock-grid floors (Context B). Baseline freezing behavior was evaluated in the first two minutes of the test. A total of 6 auditory tones (same parameters as training) were presented every minute to evaluate fear memory. Mice were returned to their home cage upon completing the fear memory test. Freezing behavior was scored automatically with Med Associates VideoFreeze software as previously described [79,93].

**Perfusions and sectioning**

Mice were euthanized 90 minutes after the fear memory retrieval test. Mice were injected with avertin (250mg/kg, i.p.) to induce deep anesthesia. Once unresponsive to tail and toe pinches, mice were transcardially perfused with 0.1M phosphate-buffered saline (PBS), followed by cold 4% paraformaldehyde fixative (PFA). The brains were extracted and stored in PFA overnight at 4°C. Brains were sectioned at 50µm (1 in 6 series) in the coronal plane with a vibratome (model VT1000, Leica). Sections were stored at -20°C in a cryoprotectant solution comprised of 60% glycerol and 0.01% sodium azide in 0.1M PBS.

**Serum corticosterone**

A separate cohort of mice with no previous behavioral testing history (n=5 per group) was used to determine the effect of DP manipulations on serum corticosterone. The DP was injected with mCherry, hM4D, or hM3D viral constructs using identical parameters to those described earlier. After a 2-week recovery period, mice were weighed and acclimated to a procedure room for at least one hour. Mice were injected with C21 (2mg/kg, 0.5mg/mL, i.p.) and immediately returned to their home cage. Mice remained in their home cage for 90 minutes undisturbed and were then euthanized as described above. Immediately prior to perfusion, blood was extracted from the heart (~0.3 to 0.5mL) with a 23-gauge needle attached to a 1mL syringe. The blood was immediately transferred to a 1.5mL Eppendorf tube and allowed to coagulate at room temperature for 30 minutes. Blood samples then underwent centrifugation to isolate serum (10,000 rpm, 10 minutes). The isolated serum was extracted with a 1mL pipette, transferred into a fresh microcentrifuge tube, and flash frozen with liquid nitrogen. Samples were stored at -20°C until use. Serum corticosterone was evaluated with a colorimetric competitive enzyme immunoassay kit (#ADI-900-097, Enzo Life Sciences) following the manufacturer's instructions. Briefly, serum samples (1 in 40 dilution) were read at 405nm with 570nm correction on a Biotek

Synergy Neo2 Multi-Mode Plate Reader (Agilent) and analyzed using Biotek Gen5 software (version 3.08, Agilent).

**Immunofluorescence**

Immunofluorescence staining was performed on free-floating sections. Sections were initially washed in 0.1M PBS and then incubated in a blocking solution containing 5% (v/v) normal goat serum and 0.25% (v/v) Triton X-100 in 0.1M PBS for 30 minutes. The mCherry viral signal was amplified by incubating sections with polyclonal rabbit anti-mCherry primary antibody (1:2000, catalog #ab167453, Abcam; RRID: AB_2571870) diluted in blocking solution. Sections were incubated overnight at 4°C on a rotary shaker under gentle agitation. On the following day, sections were washed in 0.1M PBS and then incubated in goat anti-rabbit Alexa Fluor 568 (1:500, catalog #A11011, Thermo Fisher Scientific; RRID: AB_143157) for 2hrs at room temperature. Hoechst 33342 (1:1000 diluted in 0.1M PBS, Thermo Fisher Scientific) was used as a counterstain. Sections were then rinsed in 0.1M, mounted onto gelatin-coated slides, and allowed to air dry for 30 minutes. The mounted sections were then coverslipped with Citifluor anti-fade mounting medium (catalog #17970, Electron Microscopy Sciences) and stored in a microscope slide storage book at 4°C until imaging.

To determine whether C21 modified DP activity across treatment groups, we processed a subset of PFC sections for the immediately early gene c-Fos. We chose sections from mice used in the serum corticosterone experiment because they did not undergo any behavioral testing which could influence patterns of c-Fos expression. Immunofluorescence staining for c-Fos was performed as previously described [79]. Sections were rinsed in 0.1M PBS and then incubated in 1% $H_20_2$ in 0.1M PBS to quench endogenous peroxidase activity. Sections were incubated overnight at 4°C with monoclonal rabbit anti c-Fos (1:8000, catalog #226 008, Synaptic Systems; RRID: AB_2891278) and monoclonal rat anti-mCherry (1:3000, catalog #M11217, Thermo Fisher Scientific; RRID: AB_2536611) diluted in 0.1M Tris-buffered saline and 0.5% (w/v) Roche Blocking Reagent (catalog #11096176001, Sigma-Aldrich). On the following day, sections were rinsed in 0.1M PBS and incubated in goat anti-rat Alexa Fluor 568 secondary antibody (1:500, catalog #A11077, Thermo Fisher Scientific; RRID: AB_2534121) for 1 hr. Sections were then rinsed in 0.1M PBS and incubated in donkey anti-rabbit horseradish peroxidase-conjugated secondary antibody (1:500, catalog #711-036-152, Jackson ImmunoResearch; RRID: AB_2340590) for 1hr. Tyramide signal amplification was then performed with a fluorescein tyramide conjugate (1:400) diluted in 0.1M borate buffer containing 0.01% $H_20_2$. Hoechst 33342 was used as a counterstain using the same parameters described above. Sections were then mounted onto gelatin-coated slides, air dried, and coverslipped with Citifluor anti-fade mounting medium as described above.

**Image acquisition & quantification**

Images were acquired on a Nikon Eclipse Ni-U epifluorescence microscope connected to a computer running NIS-Elements software (v 5.11.03, Nikon). Immunofluorescence signal was visualized with a LED illumination system (X-Cite 120 LED Boost, Excelitas Technologies) and 10x Plan-Apochromat objective. Images were captured with a Nikon DS-Qi2 digital camera. A total of 3 images per mouse were used to evaluate viral expression in the DP/DTT for the mCherry, hM4D-mCherry, and hM3D-mCherry cohorts. We evaluated viral expression via the mCherry tag in sections located approximately +1.9mm to +1.7mm AP (relative to bregma). Photomicrographs were superimposed on plates from the Paxinos Mouse Brain atlas and the spread of viral expression was drawn using the polygonal tool in Adobe Photoshop (version 24.1).

Quantification of c-Fos expression in the DP/DTT was performed with ImageJ Software (version 1.53e) using procedures described previously [79]. Briefly, a minimum of 3 PFC sections per subject were used to count the number of c-Fos immunoreactive cells in the DP/DTT. The average number of cells per section was calculated by summing the total number of c-Fos+ cells and dividing by the number of sections that were analyzed for each subject.

All figures were made in Adobe Photoshop. When brightness and/or contrast adjustments were made, these changes were applied to all photomicrographs.

**Slice electrophysiology**

We used slice electrophysiology to confirm the effect of C21 on hM3D- and hM4D-transfected neurons in the DP/DTT. Acute brain slices containing the mPFC were prepared from adult male and female C57BL/6J mice at least 14 days after AAV injection.

Mice were deeply anesthetized with isoflurane and decapitated. The brain was quickly removed and placed in ice-cold sucrose based cutting solution containing the following (in mM): 180 sucrose, 2.5 KCl, 1.25 $NaH_2PO_4$, 25 $NaHCO_3$, 1 $CaCl_2$, 2 $MgCl_2$, 2 $Na^+$ pyruvate and 0.4 L-Ascorbic acid with 95% $O_2$ and 5% $CO_2$. The brain was cut in the coronal plane (300 µm thick) using a vibratome (VT1000S, Leica). Brain slices containing the mPFC were allowed to recover for 30 min in a holding chamber containing a recovery solution at 30 °C, made up of 50% sucrose-based cutting solution and 50% artificial cerebrospinal fluid (ACSF). The ACSF was composed of (in mM): 120 NaCl, 2.5 KCl, 1.25 $NaH_2PO_4$, 25 $NaHCO_3$, 11 glucose, 2 $CaCl_2$, 1 $MgCl_2$, 2 $Na^+$ pyruvate and 0.4 L-Ascorbic acid with 95% $O_2$ and 5% $CO_2$. Slices then underwent an additional 30 min in regular ACSF at room temperature before patch-clamp recording. After recovery, individual slices were transferred to a submersion chamber, perfused at 2 mL/min with ACSF at room temperature, and mounted on an upright microscope (Eclipse FN1, Nikon) that was equipped with a water-immersion long-working distance objective (40x), epifluorescence filters, and an infrared video camera [DAGE IR-2000].

Current-clamp recordings were obtained from mCherry+ pyramidal neurons in layers 2/3 or 5 of the DP/DTT with borosilicate pipettes (3–5 MΩ) that were filled with intracellular solution containing the following (in mM): 126 K D-Gluconate, 5 KCl, 10 HEPES, 4 MgATP, 0.3 NaGTP, 10 Na-phosphocreatine. Electrophysiological data was acquired using a MultiClamp 700B amplifier (Molecular Devices). Signals were low-pass filtered at 2kHz and digitized at 20 kHz using a Digidata 1550A and pClamp10 software (Molecular devices). Series resistance of the recorded neurons were regularly monitored and only cells with stable series resistance (less than 20% of initial value) and stable holding current were included in the experimental data. Baseline data was acquired by measuring resting membrane potential (RMP) and the number of action potentials evoked by a long (1s) depolarizing current pulse. Somatic current pulses were calibrated in the baseline period to trigger approximately 3-4 action potentials (hM3D-mCherry$^+$) or 7-8 action potentials (hM4D-mCherry$^+$ pyramidal neurons). After 5 minutes of stable neuronal discharge induced by a somatic depolarization, C21 (1 µM, HelloBio) [94] was bath applied for at least 10 minutes, with the last 5 min being compared to the baseline period.

**Statistical analysis**

All results are presented as the mean ± standard error of the mean (SEM). Statistical comparisons were made in Prism 9.1 (GraphPad) with statistical significance ($p<0.05$) denoted on all graphs with an asterisk. For within subject comparisons, a paired t-test was used. Comparisons of independent groups were made using a one-way ANOVA, followed by Tukey's

Post Hoc test when appropriate. Parametric data with multiple comparisons were analyzed using a two-way repeated measures ANOVA, followed by Tukey's Post Hoc test with corrections for multiple comparisons. Normality of parametric datasets were confirmed by the D'Agostino and Pearson normality test (Prism 9.1). Potential sex differences were examined for each dataset using two-way ANOVAs followed by Šídák's multiple comparisons test. The individual analyses are reported in each section below. To facilitate interpretation of the data, and in the absence of major differences within and across tasks, we pooled male and female mice for each dataset, with individual data points presented as squares (males) and circles (females).

## Results

To explore the contribution of the DP/DTT to anxiety-, depression-like and fear behavior in mice, we bidirectionally modulated DP/DTT activity across a series of behavioral tasks with excitatory and inhibitory DREADDs (Figure 1A). AAV virus encoding excitatory (hM3D), inhibitory (hM4D) DREADDs or the control fluorophore mCherry were injected into the DP/DTT of C57BL/6J mice (Figure 1B). Viral expression was strongly localized to the DP/DTT across each treatment condition (Figure 1C-F).

### Chemogenetic activation of DP/DTT increases anxiety-like behavior in the open field test

We first examined the impact of manipulating DP/DTT activity on anxiety-like behavior in freely behaving mice in the OFT. Mice expressing the excitatory hM3D, inhibitory hM4D DREADD or a control mCherry virus in the DP/DTT region were injected with the agonist compound 21 (C21, 2 mg/kg) 1 hour prior to OF testing (Figure 2A-B). Chemogenetic activation of DP/DTT neurons (hM3D mice; 28.75 ± 3.30 seconds) decreased the time spent in the center zone of the OF arena compared to mCherry (56.02 ± 6.15 seconds) and hM4D mice (53.93 ± 7.38 seconds) (Figure 2C; One-way ANOVA, $F_{2,38}$ =7.795, p=0.002, Tukey's post hoc tests, hM3D versus mCherry $p$=0.002; hM3D versus hM4D $p$=0.011; mCherry versus hM4D $p$=0.965).

Minute-by-minute analysis of the time spent in the center zone of the open field arena revealed that hM3D mice spent significantly less time in the center zone at minute 2 compared to mCherry and hM4D mice and at minutes 3, 4, and 5 compared to mCherry-control mice (Figure 2D; two way-repeated measures ANOVA, $F_{2,38}$=7.795, $p$=0.002, Tukey's post hoc tests: minute 2, hM3D mice versus mCherry mice, $p$=0.047 and hM3D versus hM4D mice $p$=0.039; minute 3, 4 and 5, hM3D versus mCherry, $p$=0.03, 0.031 and 0.04 respectively).

In contrast, hM3D mice (456.8 ± 2.76 seconds) spent significantly more time in the outer zone of the open field apparatus compared to both mCherry control (434.1 ± 5.12 seconds) and hM4D mice (431.5 ± 8.027 seconds; Figure 2E, one way ANOVA, $F_{2,38}$=7.283, $p$=0.002; Tukey's post hoc tests, hM3D versus mCherry, $p$=0.007 and hM3D versus hM4D, $p$=0.006; mCherry versus hM4D, $p$=0.938). Furthermore, the total distance travelled in the open field arena was similar in all three experimental groups (Figure 2F-G, one-way ANOVA, $F_{2,38}$=2.292, $p$=0.115), suggesting that the effect of C21-mediated activation of DP/DTT neurons on anxiety-like behavior was not driven by changes in locomotor activity levels. We also screened the data for potential sex differences and found no effect of sex on the time spent in the center zone (Two-way ANOVA, $F_{1,35}$=1.065, $p$=0.309), outer zone ($F_{1,35}$=0.553, $p$=0.462), or total distance travelled ($F_{1,35}$=2.351, $p$=0.134). These data show that chemogenetic activation of the DP/DTT induces anxiety-like behavior in the OF test.

**Chemogenetic activation of DP/DTT increases anxiety-like behavior in the elevated plus maze test**

Next, we examined the effects of manipulating DP/DTT activity on anxiety-like behavior using the EPM test (Figure 3A-B). Consistent with the anxiogenic effect of DP/DTT activation observed in the OFT, hM3D mice (69.43 ± 6.48 seconds) spent less time in the open arms of the EPM apparatus compared to mCherry control (109.2 ± 10.36 seconds) and hM4D mice (110.1 ± 10.94 seconds; Figure 3C; one-way ANOVA, $F_{2,38}$=6.54, $p$=0.004, Tukey's post hoc tests, hM3D versus mCherry, $p$=0.008, hM3D versus hM4D, $p$=0.013; no difference between mCherry and hM4D mice, $p$=0.997). Further analysis showed that these differences were most pronounced during the first and third minutes of the test (Figure 3D; two-way repeated measures ANOVA, main effect of treatment $F_{2,38}$=6.545, $p$=0.004 and minute $F_{4,152}$=14.08, $p$<0.001, but no treatment by minute interaction $F_{8,152}$=0.753, $p$=0.644; Tukey's post hoc tests: minute 1, hM3D versus mCherry, p=0.008; minute 3, hM3D versus hM4D, p=0.030). Moreover, hM3D mice spent significantly more time in the closed arms of the EPM (190.2 ± 6.8 seconds) compared to mCherry control (159.5 ± 10.3 seconds) and hM4D mice (150.2 ± 10.0 seconds) (Figure 3E, one-way ANOVA, $F_{2, 38}$=5.27, $p$<0.001, Tukey's post hoc tests, hM3D versus mCherry, $p$=0.044, hM3D versus hM4D, $p$=0.013; no difference between the mCherry control and hM4D groups: $p$=0.766).

Additionally, hM3D mice displayed fewer entries to the open arms of the EPM (19.67 ± 1.57 entries) compared to hM4D mice (29.18 ± 2.57 entries; Figure 3F, one-way ANOVA, $F_{2,38}$=5.26, $p$<0.01, Tukey's post hoc test, hM3D versus hM4D, p<0.008). We saw no group differences in the number of entries to the open arm (hM3D versus mCherry, $p$=0.133; hM4D versus mCherry, $p$=0.361), closed arm ($F_{2,38}$=2.555, $p$=0.091; Figure 3G), middle platform ($F_{2,38}$=2.130, $p$=0.133; data not shown), or in the time spent in the middle platform ($F_{2,38}$=1.899, $p$=0.164; data not shown). All three experimental groups showed equivalent total distance travelled in the EPM apparatus (Figure 3H, one-way ANOVA, $F_{2,38}$=0.018, p=0.98). We found no sex differences in the time spent in the open arms ($F_{1,35}$=2.714, $p$=0.108), time spent in the closed arms ($F_{1,35}$=1.595, $p$=0.215), open arm entries ($F_{1,35}$=0.280, $p$=0.600), or closed arm entries ($F_{1,35}$=1.272, $p$=0.267). We found a significant effect of sex on the distance travelled in the EPM, with hM4D males travelling significantly less distance compared to hM4D females ($F_{1,35}$=10.22, $p$=0.003; Sidak's multiple comparisons test $p$=0.037; mCherry male vs female, $p$=0.337, and hM3D male vs female, $p$=0.542). Taken together, our data suggest that acute activation of DP/DTT neurons results in increased anxiety-like responses in the OFT and EPM.

**Chemogenetic activation of DP/DTT increases passive coping behavior**

To examine whether chemogenetic modulation of DP/DTT activity affects passive coping behavior, we next subjected mice to a tail suspension test (TST; Figure 4A-B). hM3D mice spent significantly more time immobile (66.45 ± 1.45%) compared to mCherry (57.25 ± 2.92%) and hM4D (55.00 ± 3.75%) groups following C21 injection (Figure 4D, one-way ANOVA, $F_{2,38}$=5.07, $p$=0.11; Tukey's post hoc tests, hM3D vs mCherry, $p$=0.041, hM3D vs hM4D, $p$=0.017; mCherry versus hM4D p=0.838), consistent with increased passive coping in the hM3D group.

Minute-by-minute analysis of immobility revealed a significant main effect of treatment on immobility (Figure 4E; $F_{2,38}$=5.077, $p$=0.011), but no main effect of minute ($F_{3,114}$=1.553, $p$=0.205), and no treatment by minute interaction ($F_{6,114}$=0.829, $p$=0.555). Additionally, all three groups showed equivalent length of the longest bout of immobility, and number of transitions from mobility to immobility states (Figure 4F-G, one-way ANOVAs $F_{2, 38}$=1.874, $p$=0.167 and $F_{2, 38}$=0.614, $p$=0.547, respectively). We found no sex differences in the TST (Two-way ANOVAs,

time immobile $F_{1,35}$=1.712, $p$=0.199; longest immobility bout $F_{1,35}$=0.061, $p$=0.807; number mobility-immobility transitions $F_{1,35}$=2.044, $p$=0.162).

To expand our findings of increased passive coping behavior in the TST following DP/DTT activation, we conducted a forced swim test (Figure 5A-B). C21 treatment did not affect time spent immobile in any of the experimental groups (Figure 5C-D, one-way ANOVA, $F_{2, 38}$=1.722, p=0.192; Figure 5E, two-way repeated measures ANOVA, no main effect of treatment on percent immobility $F_{2,38}$=1.723, $p$=0.192, no main effect of minute $F_{3,114}$=1.266, $p$=0.289, and no treatment by minute interaction $F_{6,114}$=1.485, $p$=0.189). We then examined the impact of chemogenetic modulation of DP/DDT activity on the longest bout of immobility and the number of transitions between mobility and immobility states in the FST (Figure 5F-G). We noted a non-significant trend of treatment effect on the longest bout of immobility (Figure 5F, one-way ANOVA, $F_{2,38}$=3.22, p=0.051), but no significant effect on the number of transitions between mobility and immobility (Figure 5G, one-way ANOVA, $F_{2,38}$=1.722, p=0.192). When we analyzed sex differences, we found that hM3D females spent significantly less time immobile than hM3D males and hM4D females (Two-way ANOVA, $F_{1,35}$=6.561, $p$=0.015; Sidak's multiple comparisons test, hM3D females versus hM3D males $p$=0.0093; hM3D females versus hM4D females p=0.0482; mCherry male versus female, $p$=0.264; hM4D male versus female, $p$=0.998). We did not observe any sex differences in the longest bout of immobility ($F_{1,35}$=2.696, $p$=0.107), or the number of mobility-immobility transitions ($F_{1,35}$=3.369, $p$=0.075). Taken together, our results demonstrate that activation of DP/DTT neurons promotes passive coping behavior in the TST, but do not alter behavior in the FST in mice.

**Chemogenetic inhibition of DP/DTT activity slightly facilitates auditory fear acquisition, but does not affect retrieval**

The inhibition of the DP/DTT-DMH pathway blocks stress-induced avoidance behavior [68]. Based on this finding, we next sought to explore whether manipulating DP/DTT activity might affect fear memory. To test this, we inhibited or activated the DP/DTT one hour prior to training mice to associate an auditory tone (conditioned stimulus: CS) with an electric foot shock (unconditioned stimulus: US, Figure 6A). During fear acquisition, chemogenetic manipulation of DP/DTT activity did not affect baseline freezing (one-way ANOVA, $F_{2,38}$=2.367, $p$=0.107; data not shown), or the mean percent freezing across all tones (Figure 6B, one-way ANOVA, $F_{2,38}$=2.828, $p$=0.072). However, we found that hM4D mice displayed a right shift in their fear learning curve, with significantly higher freezing during tone 4 and 6 of the training protocol compared to hM3D mice (Figure 6C, two-way repeated measures ANOVA, no main effect of treatment $F_{2,38}$=2.828, $p$=0.072, but significant effect of tone $F_{5,190}$=100.6, $p$<0.001, and no treatment by tone interaction $F_{10,190}$=1.633, $p$<0.099; Tukey's post hoc tests, minute 4 hM3D versus hM4d, $p$=0.012, and minute 6 hM3D versus hM4D, $p$=0.012) suggesting a slight facilitation of auditory fear acquisition upon DP/DTT inhibition.

DP/DTT manipulation did not affect post-shock freezing (Figure. 6D, One-way ANOVA, $F_{2, 38}$=0.403, $p$=0.671; Figure 6E, two-way repeated ANOVA, $F_{2, 38}$=0.46, $p$=0.635). We found a significant effect of sex on average freezing to tone (Two-way ANOVA, $F_{1,35}$=7.786, $p$=0.009) and post-shock freezing (Two-way ANOVA, F1,35=7.72, p=0.009), but post hoc tests found no significant differences between males and females within any of the groups (Sidak's multiple comparisons test, average tone freezing: mCherry $p$=0.126, hM3D $p$=0.351, hM4D $p$=0.505; post-shock freezing mCherry p=0.999, hM3D p=0.625, hM4D p=0.348; no sex differences in baseline freezing: two-way ANOVA, $F_{1,35}$=0.179, $p$=0.675).

Auditory fear memory retrieval was evaluated 24h later in a different context (Figure 6A). All three experimental groups showed similar baseline freezing (one-way ANOVA, $F_{2,38}$=0.153,

p=0.858; data not shown), and equivalent freezing to the tones (Figure 6F; one-way ANOVA, $F_{2,38}$ =0.507, p=0.607). Tone-by-tone analysis (Figure 6G) showed no main effect of treatment (Two-way repeated measures ANOVA, $F_{2,38}$=0.507, $p$=0.607), but a significant main effect of tone ($F_{5,190}$=4.00, $p$=0.002, no treatment by tone interaction: $F_{10,190}$=1.213, $p$=0.285), likely driven by within-session extinction. DP/DTT manipulation did not affect post-tone freezing (Figure 6H, average freezing: one-Way ANOVA, $F_{2,38}$=0.106, $p$=0.900; Figure 6I, tone-by-tone: Two-way repeated measures ANOVA, $F_{5,190}$=2.018, p=0.078). We found no sex differences in this dataset (Two-way ANOVA, average baseline freezing $F_{1,35}$=0.397, $p$=0.533, average tone freezing $F_{1,35}$=0.075, $p$=0.786, average post-tone freezing $F_{1,35}$=0.362, $p$=0.551). Overall, these data suggest that manipulating DP/DTT activity has no major impact on auditory fear conditioning, except for a marginal facilitation of fear acquisition following DP/DTT inhibition.

**Chemogenetic activation of DP/DTT increases serum corticosterone levels**

Given the important role of the mPFC in regulating the hypothalamo-pituitary-adrenal (HPA) axis response to emotional stress [72,95–97], and the regulation of stress-induced sympathetic responses by the DP/DTT [68], we next tested the effects of DP/DTT chemogenetic modulation on serum levels of the stress hormone corticosterone. We injected C21 into a subset of mCherry, hM3D, and hM4D mice that remained in their home cage, and subsequently extracted blood to evaluate serum corticosterone (Figure 7A). Notably, these mice had not undergone any previous behavioral testing. Interestingly, hM3D mice displayed higher serum corticosterone levels (161.2 ± 18.52 ng/mL) compared to mCherry control mice (91.38 ± 12.56 ng/mL) (Figure 7B, one-way ANOVA, $F_{2, 12}$=6.325, p=0.013, Tukey's post hoc tests, hM3D versus mCherry, $p$=0.011). Chemogenetic inhibition of DP/DTT activity (116.5 ± 9.66 ng/mL) did not affect baseline serum corticosterone levels (hM4D vs mChery, $p$=0.440, hM4D vs hM3D, $p$=0.103). These data indicate that activation of DP/DTT neurons is sufficient to trigger a neuroendocrine stress response by increasing plasma corticosterone levels.

**Validation of DP/DTT chemogenetic manipulations**

To confirm that the DREADD agonist C21 influenced hM4D and hM3D mice, we first evaluated the expression of the immediate-early gene c-Fos in the subset of mice used for serum corticosterone experiments (Figure 7C). C21 administration resulted in a significant and robust induction of c-Fos expression in the DP/DTT of hM3D mice relative to mCherry and hM4D mice, and a significant decrease in c-Fos expression in the DP/DTT of hM4D mice relative to mCherry control mice (Figure 7C-D, one-way ANOVA, $F_{2,12}$=143.9, $p$<0.001, Tukey's post hoc tests, hM3D versus mCherry, $p$<0.001; hM3D versus hM4D, $p$<0.001; hM4D versus mCherry, $p$=0.030). These results confirm that acute chemogenetic activation and inhibition of DP/DTT neurons increases and decreases DP/DTT neuronal activity, respectively.

Finally, we conducted whole-cell patch clamp recordings from layers 2/3 and 5 pyramidal cells in slices from the DP/DTT region of mice two weeks after viral injection (Figure 8A-B). Bath application of C21 resulted in a significant increase in spike number in hM3D-mCherry$^+$ pyramidal neurons compared to baseline (Figure 8C-D, $t_{10}$=4.604, $p$=0.001, paired t-test) and in the depolarization of the resting membrane potential (RMP; Figure 8E, paired t-test, $t_{10}$=2.77, $p$=0.02). In contrast, C21-mediated activation of hM4D receptors resulted in a significant decrease in spike number (paired t-test, $t_5$=3.42, $p$=0.019) and in the hyperpolarization of hM4D-mCherry$^+$ pyramidal neuron resting membrane potential (Figures 8F-H; paired t-test, $t_5$=3.24, $p$=0.023). These results confirm that acute C21-mediated activation of hM3D or hM4D-expressing pyramidal cells increases and decreases their excitability, respectively.

## Discussion

Here we examined the effects of bidirectionally modulating the activity of DP/DTT neurons to anxiety-, depression-like and fear behavior in stress-naïve mice. We found that chemogenetic activation of the DP/DTT reduced the time spent in the center zone of the OFT and in the open arms of the EPM. DP/DTT activation also increased passive coping in the TST, but did not affect behavior in the FST. DP/DTT inhibition led to a slight facilitation of freezing during fear training with no impact on subsequent fear retrieval. Interestingly, DP/DTT activation led to an increase in serum corticosterone levels, suggesting the DP/DTT also modulates HPA axis activity.

Originally ascribed as part of the olfactory peduncle in the rat [98], later studies defined the DP as bordered rostrally by the orbital cortex, caudally by the genu of the corpus callosum, dorsally by the IL and ventrally by the DTT [67], consistent with its representation in Watson and Paxinos [99,100]. Tracing studies identified downstream projections from the DP spanning the thalamus (anteromedial, mediodorsal, and nucleus reuniens), insular cortex, septum, amygdala, ventral tegmental area, brainstem (periaqueductal gray, raphe nuclei, solitary tract nucleus, parabrachial nucleus and trigeminal mesencephalic nucleus), medial mamillary nucleus, and lateral hypothalamic area [33,67,101,102]. Kataoka and colleagues had identified a role for DP/DTT downstream projections to the DMH in regulating sympathetic responses and social avoidance following social defeat stress in rats [68]. Importantly, Chen and colleagues demonstrated that IL downstream projections to the lateral septum and CeA exert opposing effects on anxiety [60], suggesting a high degree of specialization within the vmPFC for anxiety-like behavioural modulation. As such, further work is necessary to determine whether DP-mediated modulation of anxiety-like behavior relies on projections to the DMH or other targets. Importantly, while many of the brain regions projecting to the DP [68] regulate anxiety-like behavior in rodents, including the mediodorsal (MD) [103–106] and paraventricular (PVT) [107–111] thalamus, insular cortex (IC) [111–116], nucleus reuniens [117] and amygdala [23,118–122], how these upstream regions influence DP/DTT activity and modulation of anxiety-like behavior remains unknown.

A considerable body of work implicates the rodent mPFC in the regulation of anxiety-like behavior [7,13,23–30,123,14–21], with contradictory findings supporting anxiogenic [14,15,27–30,53–55] or anxiolytic [16–19] roles. Manipulations selective to the vmPFC/IL also see conflicting effects on EPM and open field performance [16,18,30,60]. Recently, Chen and colleagues found that optogenetic activation of IL soma drives anxiety-like behavior in the EPM and open field [60], similar to our data with DP/DTT activation. In contrast, they found that optic stimulation of the DP increases entries to the open arms in the EPM and time spent in the center of the open field [60], contrary to our findings. Our data support an anxiogenic role for the DP/DTT, which is in line with findings from Kataoka and colleagues showing that inhibition of the DP/DTT pathway abolishes stress-induced avoidance behavior [68], and our finding of increased serum corticosterone following DP/DTT activation. Importantly, the viral spread over the DP in the study by Chen and colleagues is more dorsal (spreading to IL and the dorsal part of DP, but not DTT) compared to ours, and targets glutamatergic neurons under the αCAMKII promoter [60], in contrast to the pan-neuronal synapsin and EF1a promoters used in this and the study by Kataoka and colleagues [68]. These discrepancies suggest the possibility of additional cell-type and subregion specialization across the dorso-ventral axis of the vmPFC, and raise important questions on a potential interaction between the dorsal and ventral parts of the mPFC in regulating anxiety-like behavior and neuroendocrine responses.

Optogenetic stimulation of the DP/DTT-DMH pathway in stress-naïve animals drives sympathetic responses mimicking those triggered by social defeat stress [68], suggesting that the DP/DTT might transduce stress responses from upstream corticolimbic regions toward downstream autonomic and behavioral/motor responses [68]. Consistent with that hypothesis, we found that chemogenetic activation of DP/DTT triggers an increase in serum corticosterone levels. This is in line with another study showing that electrical stimulation of the frontal cortex increases baseline corticosterone levels [124]. Importantly, while most of the literature supports an inhibitory effect of the mPFC over HPA secretory responses following stress [71,125–128] (but see [129]), Radley and colleagues saw a dichotomy between the dorsal and ventral mPFC in modulating stress-induced HPA activation [72]. Specifically, while dorsal mPFC lesion increased corticosterone levels following acute restraint stress, ventral mPFC lesions decreased corticosterone levels [72]. This suggests that mPFC inhibition of the HPA axis response is mostly driven by the dorsal mPFC, with the ventral portion of the mPFC (possibly spanning the DP/DTT) exerting the opposite effect, consistent with our findings. Importantly, while Kataoka and colleagues saw marked effects of DP/DTT inhibition on stress-induced sympathetic responses, they saw no evidence of DP/DTT inhibition affecting basal autonomic homeostasis [68], consistent with our lack of effects of DP/DTT inhibition in stress-naïve animals. Similarly, inhibition of the ventral portion of the PFC did not affect baseline corticosterone levels [72]

The hypothalamus is necessary for the effects of frontal cortex stimulation on HPA activity [124], and mediates the autonomic effects of DP activation [68]. It is hypothesized that (dorsal) mPFC inhibition of HPA activity occurs through stimulation of GABAergic projections from DMH to the paraventricular nucleus of the hypothalamus (PVN) [130]. The ventral portion of the mPFC projects to hypothalamic nuclei sub-PVN, DMH and lateral hypothalamus (LH) [126]. Both sub-PVN and DMH project to and modulate PVN activity [126]. While Radley and colleagues proposed that the stimulating effects of ventral mPFC on HPA activity might be mediated through connections with BNST [72], studies suggest an inhibitory effect of the BNST over HPA activity following acute stress [131], and fail to see recruitment of mPFC-BNST projections following stress [128,132]. While we see weak DP projections to the BNST, the exact downstream regulation of DP/DTT effects on HPA secretory activity is unclear. Interestingly, studies consistently show that the effects of mPFC lesions on acute stress-induced HPA modulation is stress type-specific, driven by restraint [71,72,125,127,129], new cage stress [126] and immune challenge [128]; but not ether [71,125] or noise [128]. Given the more recent characterization of the role of the DP/DTT-DMH projection in mediating psychosocial stress [68], future studies should shed light on the mechanisms underlying differential regulation of stress through mPFC and DP/DTT pathways.

DP/DTT activation increased immobility time in the TST, but not in the FST. Given the differential implications of animal weight on water-based (FST) and suspension (TST) task demands, it is possible that the relatively high weight of our animals at the time of testing (>30g for males) contributed to the differences in performance between these tasks. The mPFC has a well-established role in modulating depression-like behavior [133] in both stress-naïve [56–59,134,135] and stress conditions [134,136–141], including IL-specific manipulations [57,59]. Interestingly, Warden and colleagues identified mPFC neuronal population coding for FST active and inactive behavioral states during the FST, which reflected specialization within mPFC downstream projections to the dorsal raphe nucleus and lateral habenula [142]. Accordingly, somatic activation of the mPFC as a whole did not affect behavior in the FST [142], suggesting that the probing of specific DP/DTT projections might modulate passive coping in this task and better explain our negative findings. While studies identified a role for mPFC downstream projections to the nucleus accumbens (NAc), dorsal raphe nucleus and lateral habenula in underlying changes in depression-like behavior [134,138,139,142,143], the pattern of DP/DTT

downstream targets [33,67,101,102] suggests our effects on passive coping in the TST may be driven by a different downstream effector or modulator.

Our data showed no effects of DP/DTT manipulation on auditory fear retrieval, but a slight increase in freezing during fear acquisition upon DP/DTT inhibition. Given the important role of the IL and its projections in fear extinction [60–62,144–148], a potential contribution of the DP/DTT to extinction learning remains to be explored. Although we have not seen major sex differences in the behaviors explored here, one study reported sex-specific increased recruitment of the DP in female mice following auditory fear conditioning [149]. Due to the well documented sex and gender differences in the prevalence of anxiety and posttraumatic stress (PTSD) disorders [150–152], as well as in sympathetic and autonomic function [153–156], this raises the intriguing possibility of sex differences in the long-term consequences of stress-induced activation of DP pathways. Finally, the involvement of somatostatin interneurons in the dorsomedial prefrontal cortex in anxiety-like [20,157] and fear [158–160] behavior, as well as vmPFC parvalbumin interneurons in anxiety- and depression-like behavior [161,162], including in the DP [162], points to the importance of exploring DP/DTT microcircuit dynamics in this context.

Overall, our data expand an emerging literature examining the contributions of the DP/DTT to the modulation of psychosocial stress and sympathetic responses by revealing the DP/DTT as a regulator of anxiety-like and passive coping behavior. As its topography allows for the integration of higher order information toward autonomic and sympathetic effectors, whose disfunction is often a feature of anxiety disorders, the DP/DTT may be uniquely placed to mediate the effects of stress on affective function. Our findings support further specialization across the dorsoventral axis of the mPFC in the processing of anxiety- and depression-like behavior and stress responsivity, in line with rising evidence of pathway-specific modulation of anxiety-like behavior among mPFC subregions.

**Acknowledgements:**
We thank Hathairat Chanphao, Tejnarine Persaud, Bebhinn Treanor, and Christina Guzzo for their generous and fundamental assistance with the corticosterone ELISA experiment and use of the Guzzo lab plate reader. We would also like to thank Unza Mumtaz and Mehreen Inayat for their help with animal colony management. Some figure diagrams were created with the assistance of BioRender.com.

**Author Contributions:**
*Designed Research:* JJB, AK, MAC.
*Performed Research:* JJB, AK, RA, ACS, HP
*Analyzed/Interpreted Data:* JJB, AK, MAC.
*Wrote the paper:* JJB, AK, MAC.
All authors reviewed and approved the manuscript.

**Conflict of Interest Statement:**
The Authors declare no competing financial interests.

**Funding Sources:**
This work was supported by grants from CIHR (PJT 399790), Human Frontier Science Program Organization (CDA00009/2018 and RGY0072/2019), the SickKids Foundation and Canadian Institutes of Health Research (CIHR) – Institute of Human Development, Child and Youth Health (NI19-1132R), and Natural Sciences and Engineering Research Council of Canada (RGPIN-2017-06344) to MAC.

**Figures:**
8 primary

**Word counts:**
*Abstract: 259*
*Introduction: 516*
*Discussion: 1543*

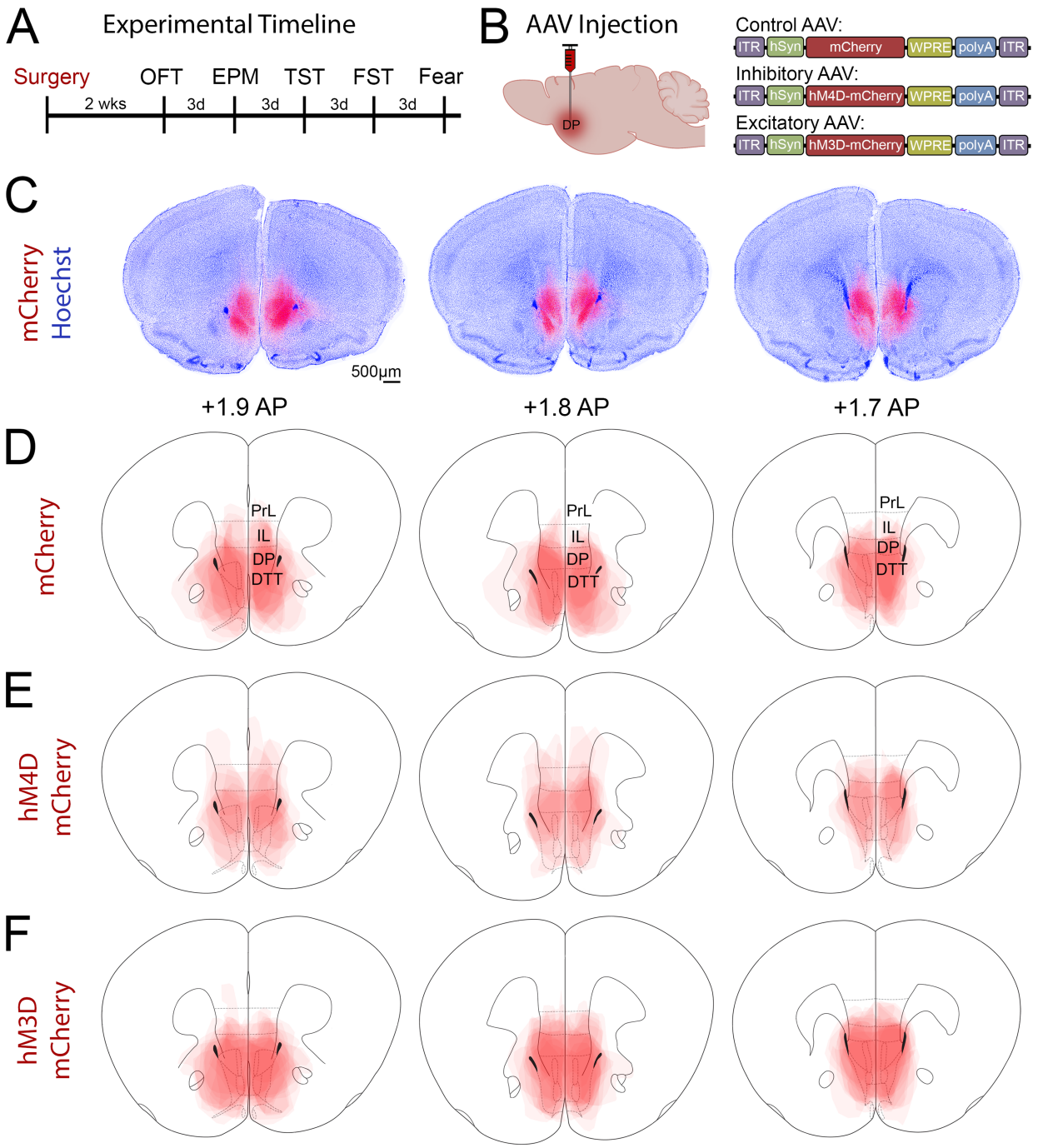


**Figure 1. Viral expression in the DP/DTT**

**A-B.** Experimental timeline. C57BL/6J mice were injected with AAV5-hSyn-mCherry, AAV5-hSyn-hM3D-mCherry or AAV5-hSyn-hM4D-mCherry into the DP/DTT. Following 2 weeks, mice underwent a battery of behavioral tests comprised of the open field test (OFT), elevated plus maze (EPM), tail suspension test (TST), forced swim test (FST) and auditory fear conditioning (Fear) with a washout period of three days between each test. **C.** Representative images of an mCherry control virus-infused brain stained for mCherry (red) and the nuclear dye Hoechst (blue). **D-F.** Diagrams depicting overlaid viral spread for all mCherry (**D**), hM4D (**E**) and hM3D-injected (**F**) mice. Scale bar = 500µm.

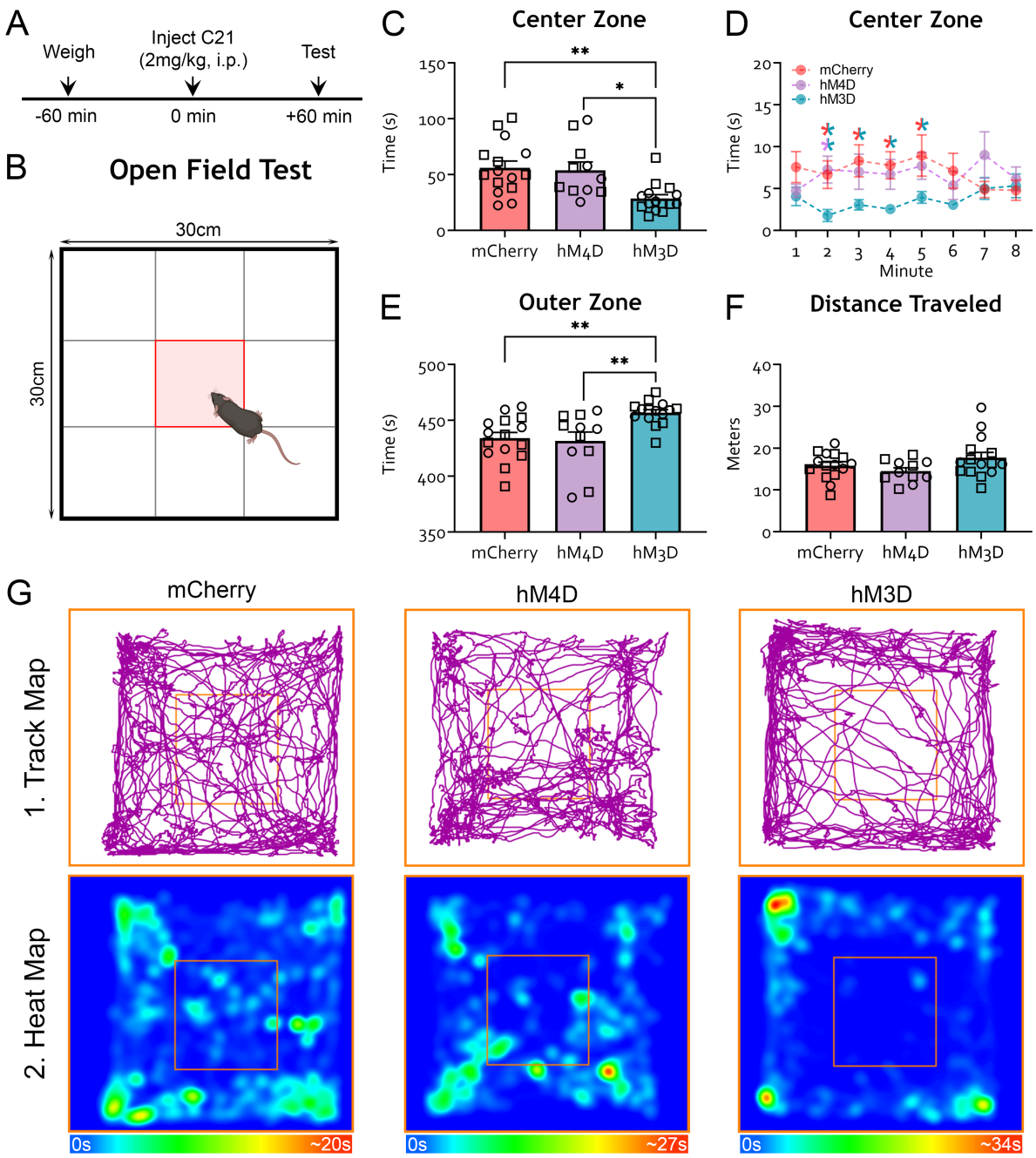


**Figure 2. Chemogenetic activation of the DP/DTT increases anxiety-like behavior in the open field test.** **A-B.** Experimental timeline. Mice previously injected with hM3D, hM4D or control mCherry constructs in the DP/DTT were injected with the DREADD agonist C21 one hour prior to being placed in an open field. The time spent in the center zone (red) and the outer zone (white) was measured. **C.** The time spent in the center zone of the open field was significantly reduced in hM3D mice compared to mCherry and hM4D mice. **D.** Time spent in the center of the open field arena was significantly reduced in hM3D mice compared to mCherry mice during minutes 2, 3, 4, and 5. The hM3D mice also spent less time in the center of the arena compared to hM4D mice during minute 2. **E.** The amount of time spent in the outer zone of the open field arena was significantly greater in the hM3D mice compared to mCherry and hM4D mice. **F.** The total distance travelled during the test did not differ between groups. **G1-2.** Representative track and heat maps. *p<0.05, **p<0.01. * indicates a significant difference between hM3D and mCherry groups; * indicates a significant difference between hM3D and hM4D groups. Male (square) and female (circle) individual datapoints are displayed for transparency (see text for details).

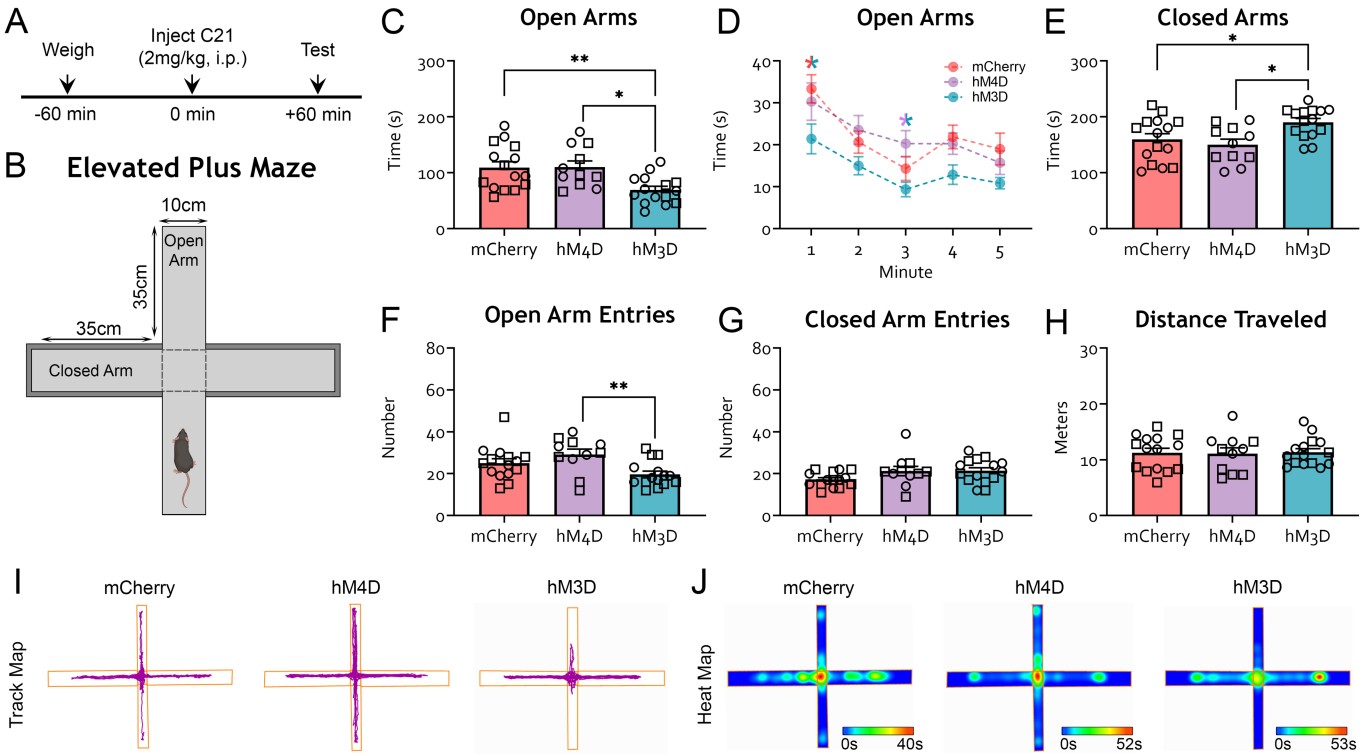


**Figure 3. Chemogenetic activation of the DP/DTT increases anxiety-like behavior in the elevated plus maze. A-B.** Experimental timeline. Mice previously injected with hM3D, hM4D or control mCherry constructs in the DP/DTT were injected with the DREADD agonist C21 one hour prior to being placed in an elevated plus maze. The time spent in the open arms vs closed arms was measured. **C.** The time spent in the open arms of the elevated plus maze was significantly reduced in hM3D mice compared to mCherry and hM4D mice. **D.** hM3D mice spent significantly less time in the open arms of the elevated plus maze compared to mCherry mice (minute 1) and hM4D mice (minute 3). **E.** The amount of time spent in the closed arms of the elevated plus maze was significantly greater in the hM3D mice compared to mCherry and hM4D mice. **F.** The number of open arm entries was significantly reduced in hM3D mice compared to hM4D mice. **G.** The number of closed arm entries during the test did not differ between groups. **H.** The total distance travelled during the test did not differ between groups. While we found that hM4D males travelled less than hM4D females (see results), separation of the data by sex did not reveal group differences (One-way ANOVA, females $F_{2,16}$= 0.3571, p= 0.7051; males $F_{2,19}$= 0.4524, p= 0.6427). **I-J.** Representative track and heat maps. *p<0.05, **p<0.01. * indicates a significant group difference between mCherry and hM3D conditions; * indicates a significant group difference between hM3D and hM4D conditions. Male (square) and female (circle) individual datapoints are displayed for transparency (see text for details).

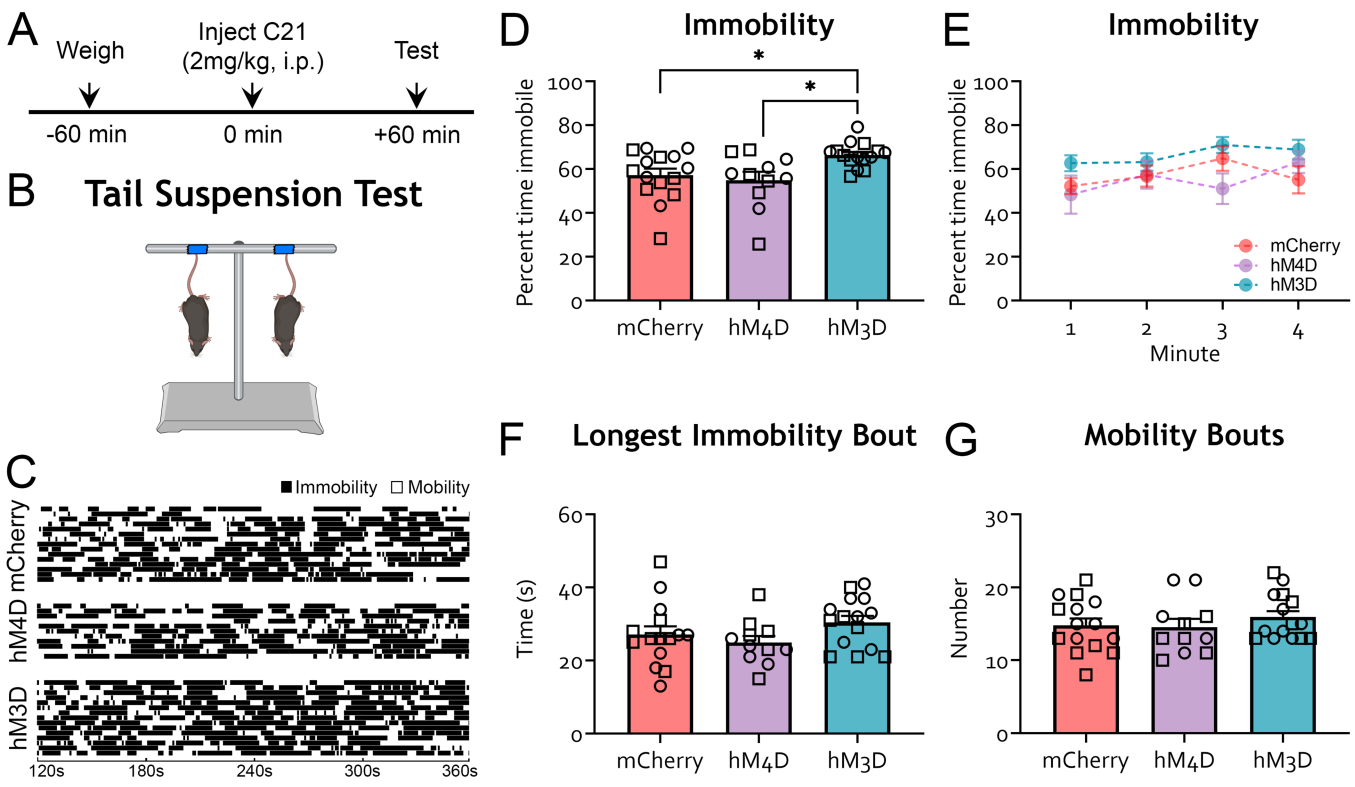


**Figure 4. Chemogenetic activation of the DP/DTT increases immobility in the tail suspension test.** **A-B.** Experimental timeline. Mice previously injected with hM3D, hM4D or control mCherry constructs in the DP/DTT were injected with the DREADD agonist C21 one hour prior to undergoing the tail suspension test. **C.** Representative raster plots for each mouse indicating periods of immobility (black) and mobility (white) over the tail suspension test duration. **D.** The average percent of time spent immobile during the TST was significantly greater in hM3D mice compared to mCherry and hM4D mice. **E.** A two-way repeated measures ANOVA found no group differences during any minute of the test. **F.** The longest continuous period of immobility did not differ between groups. **G.** The number of mobility-immobility transitions (mobility bouts) did not differ between groups. *p<0.05. Male (square) and female (circle) individual datapoints are displayed for transparency (see text for details).

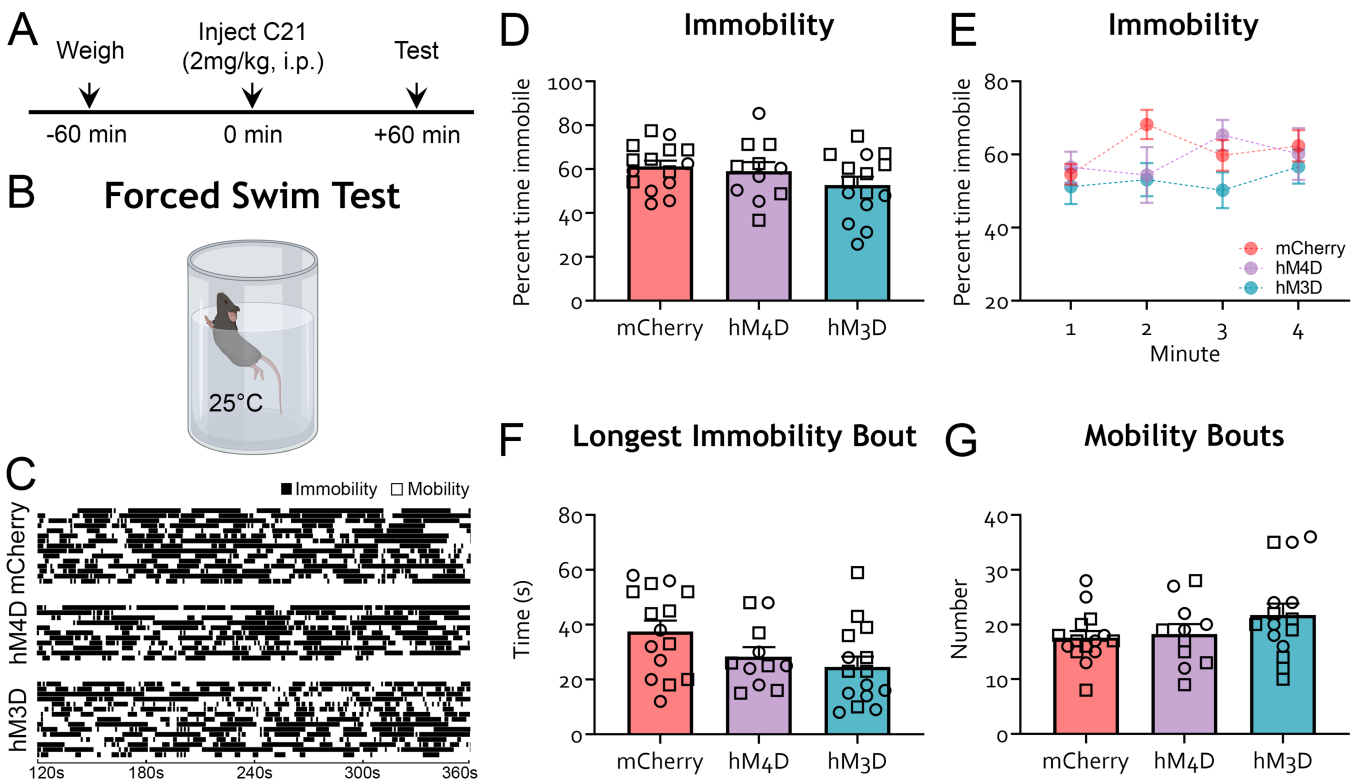


**Figure 5. Chemogenetic manipulations of the DP/DTT have no effect on forced swim behaviors.** **A-B.** Experimental timeline. Mice previously injected with hM3D, hM4D or control mCherry constructs in the DP/DTT were injected with the DREADD agonist C21 one hour prior to undergoing the forced swim test. **C.** Representative raster plots for each mouse indicating periods of immobility (black) and mobility (white) over the forced swim test duration. **D.** There was no effect of treatment on percent immobility in the forced swim test. While we found that hM3D females had a lower percent time spent immobile compared to males (see results), separation of the data by sex did not reveal group differences (One-way ANOVA, females $F_{2,16}$= 2.816, p= 0.0896; males $F_{2,19}$=1.042, p= 0.3722). **E.** Percent immobility did not differ between groups. **F.** The longest continuous period of immobility did not differ between groups. **G.** The number of mobility-immobility transitions (mobility bouts) did not differ between groups. *p<0.05. Male (square) and female (circle) individual datapoints are displayed for transparency (see text for details).

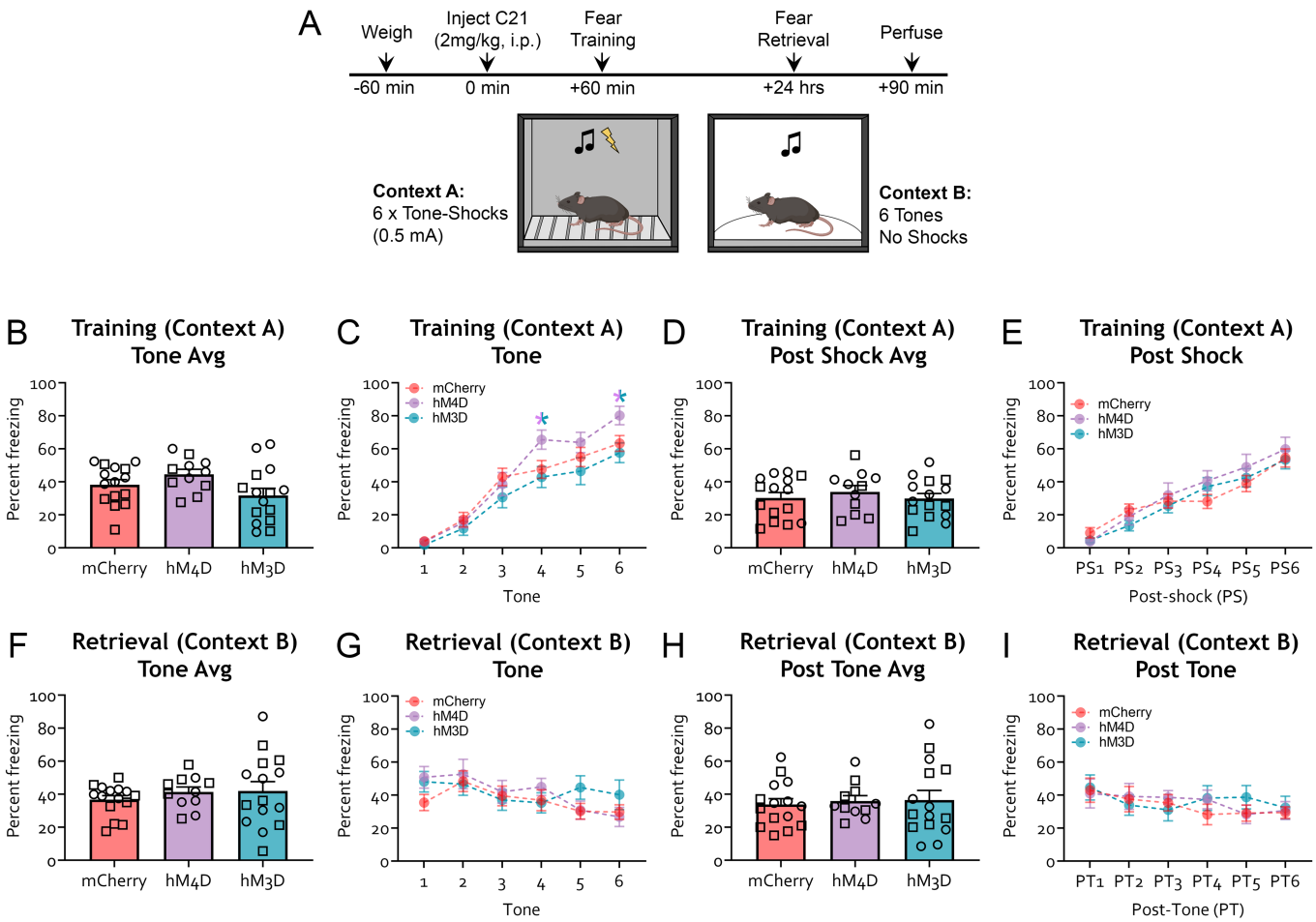


**Figure 6. Chemogenetic manipulations of the DP/DTT have modest effects on auditory fear acquisition and no effect on fear memory retrieval.**

**A.** Experimental timeline. Mice previously injected with hM3D, hM4D or control mCherry constructs in the DP/DTT were injected with the DREADD agonist C21 one hour prior to undergoing auditory fear conditioning. During acquisition, mice were placed in a sound-attenuated fear conditioning chamber and received 6 tone-shock pairings (0.5mA). Twenty-four hours later, auditory fear memory was evaluated in a different context in the absence of shocks. **B.** During fear acquisition, DP/DTT manipulations did not affect average tone freezing. **C.** hM4D mice displayed significantly more freezing than hM3D mice at tone presentations 4 and 6 during acquisition. **D-E.** DP/DTT manipulations did not affect average or individual post shock freezing episodes. **F-I.** During fear retrieval, DP/DTT manipulations did not affect freezing during average tone (**F**), individual tone (**G**), average post tone (**H**) or individual post tone (**I**) periods. * indicates a significant difference between hM3D and hM4D groups ($p<0.05$). Male (square) and female (circle) individual datapoints are displayed for transparency (see text for details).

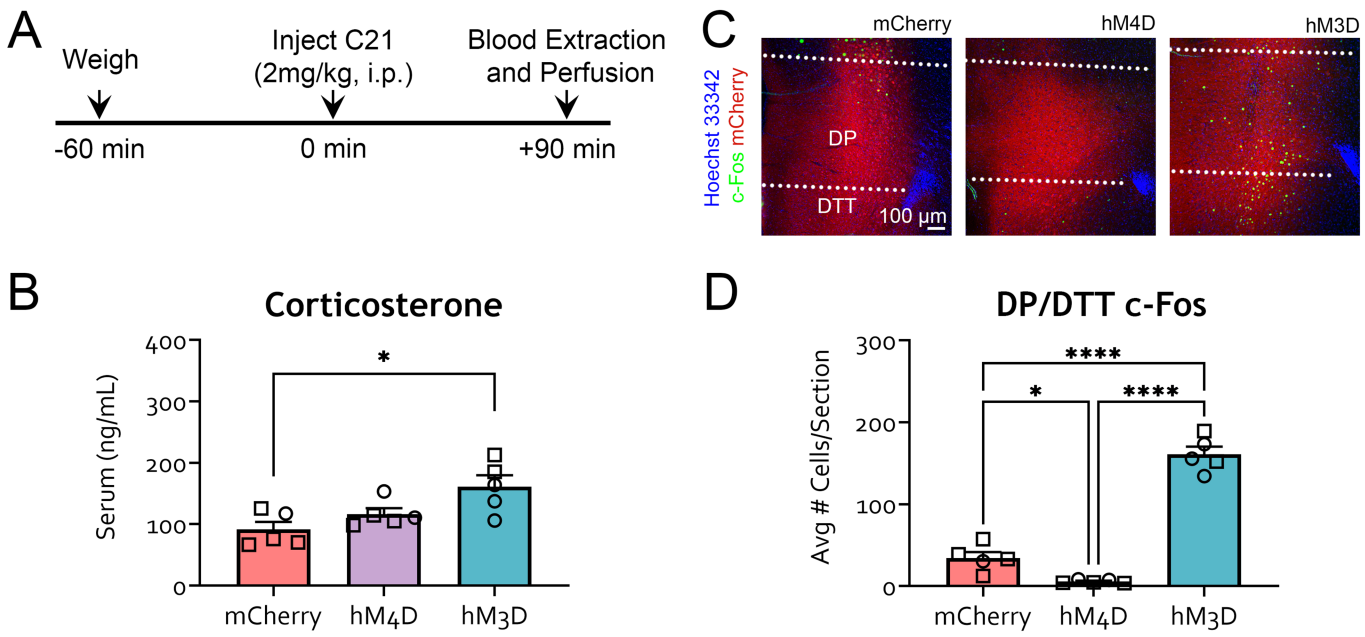


**Figure 7. Chemogenetic activation of the DP/DTT increases serum corticosterone and c-Fos expression.** **A.** Experimental timeline. Mice previously injected with hM3D, hM4D or control mCherry constructs in the DP/DTT were injected with the DREADD agonist C21 and euthanized 90 minutes later. Blood was extracted at the time of perfusion for corticosterone measurements. **B.** Serum corticosterone was significantly higher in hM3D mice compared to mCherry mice. **C.** Representative photomicrographs showing c-Fos (green) and mCherry (red) expression in the DP/DTT following C21 treatment. Note the significant number of c-Fos$^{+}$ neurons in the hM3D mice. Hoechst 33342 (blue) was used as a nuclear marker. The lateral ventricle (dense blue stain on the right of each photomicrograph) was used as a landmark for the DP/DTT. **D.** hM3D mice had significantly more c-Fos+ neurons in the DP/DTT than mCherry and hM4D mice. Furthermore, mCherry mice also had significantly more c-Fos+ neurons in the DP than hM4D mice. *$p<0.05$, ****$p<0.0001$. Scale bar: 100µm. Male (square) and female (circle) individual datapoints are displayed for transparency.

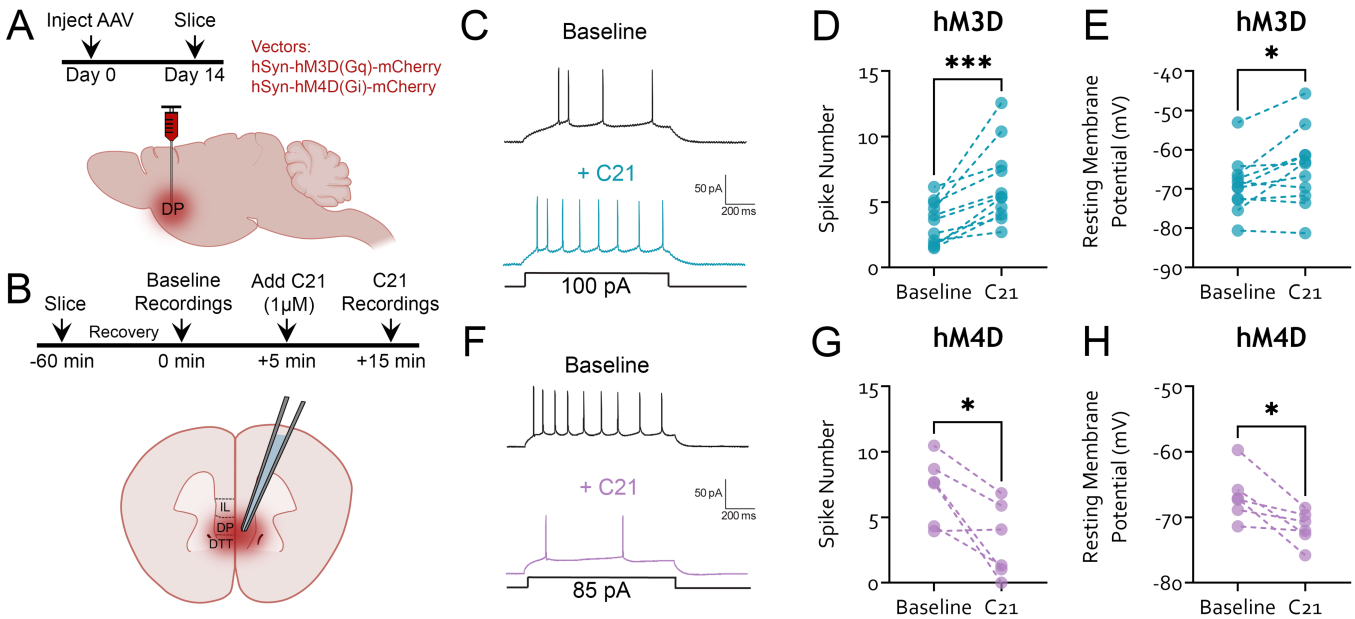


**Figure 8. Confirmation of C21 effects on hM3D⁺ and hM4D⁺ pyramidal neurons in the DP/DTT.** **A.** Experimental design. AAV constructs encoding hM3D-mCherry or hM4D-mCherry were injected into the DP and slices were made at least 14 days later. **B.** Experimental timeline for electrophysiological recordings. Slices were made and allowed to recover for 60 minutes prior to collecting baseline recordings in mCherry⁺ neurons. After a stable baseline recording of depolarization-induced firing, C21 (1 μM) was bath applied for at least 10 minutes and the last 5 minutes of the recording period were compared to the baseline. **C.** Representative traces of action potentials recorded from an hM3D⁺ neuron at baseline and after application of C21. **D.** The number of action potentials evoked by somatic current injection (100pA) in hM3D⁺ transfected neurons was significantly increased following bath application of C21 (n=11 cells, 4 mice). **E.** The resting membrane potential (RMP) of hM3D⁺ neurons became significantly more depolarized following bath application of C21. **F.** Representative traces of action potentials recorded from an hM4D⁺ neuron at baseline and after application of C21. **G.** The number of action potentials evoked by somatic current injection (85pA) in hM4D⁺ neurons was significantly decreased following bath application of C21 (n=6 cells, 3 mice). **E.** The RMP of hM4D⁺ neurons became significantly more hyperpolarized following bath application of C21. *p<0.05, ***p<0.001

**References:**


1. Knight RT, Grabowecky MF, Scabini D. Role of human prefrontal cortex in attention control. Adv Neurol. 1995;66:21–26.

2. Rossi AF, Pessoa L, Desimone R, Ungerleider LG. The prefrontal cortex and the executive control of attention. Exp Brain Res. 2009;192:489–497.

3. Bechara A, Tranel D, Damasio H. Characterization of the decision-making deficit of patients with ventromedial prefrontal cortex lesions. Brain. 2000;123 ( Pt 1:2189–2202.

4. Euston DR, Gruber AJ, McNaughton BL. The role of medial prefrontal cortex in memory and decision making. Neuron. 2012;76:1057–1070.

5. Bahmani Z, Clark K, Merrikhi Y, Mueller A, Pettine W, Isabel Vanegas M, et al. Prefrontal Contributions to Attention and Working Memory. Curr Top Behav Neurosci. 2019;41:129–153.

6. Vogel P, Hahn J, Duvarci S, Sigurdsson T. Prefrontal pyramidal neurons are critical for all phases of working memory. Cell Rep. 2022;39:110659.

7. Yizhar O, Fenno LE, Prigge M, Schneider F, Davidson TJ, Shea DJO, et al. Neocortical excitation / inhibition balance in information processing and social dysfunction. Nature. 2011;477:171–178.

8. Ko J. Neuroanatomical Substrates of Rodent Social Behavior: The Medial Prefrontal Cortex and Its Projection Patterns. Front Neural Circuits. 2017;11:41.

9. Yizhar O, Levy DR. The social dilemma: prefrontal control of mammalian sociability. Curr Opin Neurobiol. 2021;68:67–75.

10. Kuga N, Abe R, Takano K, Ikegaya Y, Sasaki T. Prefrontal-amygdalar oscillations related to social behavior in mice. Elife. 2022;11.

11. Etkin A, Egner T, Kalisch R. Emotional processing in anterior cingulate and medial prefrontal cortex. Trends Cogn Sci. 2011;15:85–93.

12. Price JL, Drevets WC. Neural circuits underlying the pathophysiology of mood disorders. Trends Cogn Sci. 2012;16:61–71.

13. Adhikari A, Topiwala M a, Gordon J a. Synchronized activity between the ventral hippocampus and the medial prefrontal cortex during anxiety. Neuron. 2010;65:257–269.

14. Cao J, Liu X, Liu JX, Zhao S, Guo YX, Wang GY, et al. Inhibition of glutamatergic neurons in layer II/III of the medial prefrontal cortex alleviates paclitaxel-induced neuropathic pain and anxiety. Eur J Pharmacol. 2022;936.

15. Parfitt GM, Nguyen R, Bang JY, Aqrabawi AJ, Tran MM, Seo DK, et al. Bidirectional Control of Anxiety-Related Behaviors in Mice: Role of Inputs Arising from the Ventral Hippocampus to the Lateral Septum and Medial Prefrontal Cortex. Neuropsychopharmacology. 2017;42:1715–1728.

16. Jinks AL, McGregor IS. Modulation of anxiety-related behaviours following lesions of the prelimbic or infralimbic cortex in the rat. Brain Res. 1997;772:181–190.

17. Pati S, Sood A, Mukhopadhyay S, Vaidya VA. Acute pharmacogenetic activation of medial prefrontal cortex excitatory neurons regulates anxiety-like behaviour. J Biosci. 2018;43:85–95.

18. Adhikari A, Lerner TN, Finkelstein J, Pak S, Jennings JH, Davidson TJ, et al. Basomedial amygdala mediates top-down control of anxiety and fear. Nature. 2015;527:179–185.

19. Yin J Bin, Liang SH, Li F, Zhao WJ, Bai Y, Sun Y, et al. dmPFC-vlPAG projection neurons contribute to pain threshold maintenance and antianxiety behaviors. J Clin Invest. 2020;130:6555–6570.

20. Soumier A, Sibille E. Opposing effects of acute versus chronic blockade of frontal cortex somatostatin-positive inhibitory neurons on behavioral emotionality in mice. Neuropsychopharmacology. 2014;39:2252–2262.

21. Calhoon GG, Tye KM. Resolving the neural circuits of anxiety. Nat Neurosci. 2015;18:1394–1404.

22. Wang GQ, Cen C, Li C, Cao S, Wang N, Zhou Z, et al. Deactivation of excitatory neurons in the prelimbic cortex via Cdk5 promotes pain sensation and anxiety. Nat Commun. 2015;6:7660.

23. Adhikari A. Distributed circuits underlying anxiety. Front Behav Neurosci. 2014.

24. Likhtik E, Stujenske JM, Topiwala MA, Harris AZ, Gordon JA. Prefrontal entrainment of amygdala activity signals safety in learned fear and innate anxiety. Nat Neurosci. 2014;17:106–113.

25. Adhikari A, Topiwala MA, Gordon JA. Single units in the medial prefrontal cortex with anxiety-related firing patterns are preferentially influenced by ventral hippocampal activity. Neuron. 2011;71:898–910.

26. Yu H, Chen L, Lei H, Pi G, Xiong R, Jiang T, et al. Infralimbic medial prefrontal cortex signalling to calbindin 1 positive neurons in posterior basolateral amygdala suppresses anxiety- and depression-like behaviours. Nat Commun. 2022;13:1–14.

27. Sullivan RM, Gratton A. Behavioral effects of excitotoxic lesions of ventral medial prefrontal cortex in the rat are hemisphere-dependent. Brain Res. 2002;927:69–79.

28. Shah AA, Treit D. Excitotoxic lesions of the medial prefrontal cortex attenuate fear responses in the elevated-plus maze, social interaction and shock probe burying tests. Brain Res. 2003;969:183–194.

29. Lacroix L, Spinelli S, Heidbreder CA, Feldon J. Differential role of the medial and lateral prefrontal cortices in fear and anxiety. Behav Neurosci. 2000;114:1119–1130.

30. Suzuki S, Saitoh A, Ohashi M, Yamada M, Oka JI, Yamada M. The infralimbic and prelimbic medial prefrontal cortices have differential functions in the expression of anxiety-like behaviors in mice. Behav Brain Res. 2016;304:120–124.

31. Sesack SR, Deutch a Y, Roth RH, Bunney BS. Topographical organization of the efferent projections of the medial prefrontal cortex in the rat: an anterograde tract-tracing study with Phaseolus vulgaris leucoagglutinin. J Comp Neurol. 1989;290:213–242.

32. Miller EK, Cohen JD. An Integrative Theory of Prefrontal Cortex Function. Annu Rev Neurosci. 2001;24:167–202.

33. Gabbott PLA, Warner TA, Jays PRL, Salway P, Busby SJ. Prefrontal cortex in the rat: Projections to subcortical autonomic, motor, and limbic centers. J Comp Neurol. 2005;492:145–177.

34. Hoover WB, Vertes RP. Anatomical analysis of afferent projections to the medial prefrontal cortex in the rat. Brain Struct Funct. 2007;212:149–179.

35. Ährlund-Richter S, Xuan Y, van Lunteren JA, Kim H, Ortiz C, Pollak Dorocic I, et al. A whole-brain atlas of monosynaptic input targeting four different cell types in the medial prefrontal cortex of the mouse. Nat Neurosci. 2019;22:657–668.

36. Anastasiades PG, Carter AG. Circuit organization of the rodent medial prefrontal cortex. Trends Neurosci. 2021;44:550–563.

37. Riga D, Matos MR, Glas A, Smit AB, Spijker S, Van den Oever MC. Optogenetic dissection of medial prefrontal cortex circuitry. Front Syst Neurosci. 2014;8:230.

38. Bittar TP, Labonte B. Functional Contribution of the Medial Prefrontal Circuitry in Major Depressive Disorder and Stress-Induced Depressive-Like Behaviors. Front Behav Neurosci. 2021;15:699592.

39. Carlén M. What constitutes the prefrontal cortex? Science (80- ). 2017;358:478–482.

40. Le Merre P, Ahrlund-Richter S, Carlen M. The mouse prefrontal cortex: Unity in diversity. Neuron. 2021;109:1925–1944.

41. Xu P, Chen A, Li Y, Xing X, Lu H. Medial prefrontal cortex in neurological diseases. Physiol Genomics. 2019;51:432–442.

42. George O, Koob GF. Individual differences in prefrontal cortex function and the transition from drug use to drug dependence. Neurosci Biobehav Rev. 2010;35:232–247.

43. Riga D, Matos MR, Glas A, Smit AB, Spijker S, Van den Oever MC. Optogenetic dissection of medial prefrontal cortex circuitry. Front Syst Neurosci. 2014;8:230.

44. Chini M, Hanganu-Opatz IL. Prefrontal Cortex Development in Health and Disease: Lessons from Rodents and Humans. Trends Neurosci. 2021;44:227–240.

45. Xu P, Chen A, Li Y, Xing X, Lu H. Medial prefrontal cortex in neurological diseases. Physiol Genomics. 2019;51:432–442.

46. Bishop S, Duncan J, Brett M, Lawrence AD. Prefrontal cortical function and anxiety: controlling attention to threat-related stimuli. Nat Neurosci. 2004;7:184–188.

47. Myers-Schulz B, Koenigs M. Functional anatomy of ventromedial prefrontal cortex: implications for mood and anxiety disorders. Mol Psychiatry. 2012;17:132–141.

48. Park J, Moghaddam B. Impact of anxiety on prefrontal cortex encoding of cognitive flexibility. Neuroscience. 2017;345:193–202.

49. Andersen SL, Teicher MH. Stress, sensitive periods and maturational events in adolescent depression. TINS. 2008;31:183–191.

50. Chai XJ, Whitfield-Gabrieli S, Shinn AK, Gabrieli JDE, Nieto Castãón A, McCarthy JM, et al. Abnormal medial prefrontal cortex resting-state connectivity in bipolar disorder and schizophrenia. Neuropsychopharmacology. 2011;36:2009–2017.

51. Blumberg HP, Stem E, Martinez D, Ricketts S, de Asis J, White T, et al. Increased anterior cingulate and caudate activity in bipolar mania. Bipolar Disord Sci Ment Heal. 2019:177–184.

52. Kenwood MM, Kalin NH, Barbas H. The prefrontal cortex, pathological anxiety, and anxiety disorders. Neuropsychopharmacology. 2022;47:260–275.

53. Shah AA, Sjovold T, Treit D. Inactivation of the medial prefrontal cortex with the GABAA receptor agonist muscimol increases open-arm activity in the elevated plus-maze and attenuates shock-probe burying in rats. Brain Res. 2004;1028:112–115.

54. Bi LL, Wang J, Luo ZY, Chen SP, Geng F, Chen YH, et al. Enhanced excitability in the infralimbic cortex produces anxiety-like behaviors. Neuropharmacology. 2013;72:148–156.

55. Saitoh A, Ohashi M, Suzuki S, Tsukagoshi M, Sugiyama A, Yamada M, et al. Activation of the prelimbic medial prefrontal cortex induces anxiety-like behaviors via N-Methyl-D-aspartate receptor-mediated glutamatergic neurotransmission in mice. J Neurosci Res. 2014;92:1044–1053.

56. Ferenczi E a., Zalocusky K a., Liston C, Grosenick L, Warden MR, Amatya D, et al. Prefrontal cortical regulation of brainwide circuit dynamics and reward-related behavior. Science (80- ). 2016;351:aac9698–aac9698.

57. Fuchikami M, Thomas A, Liu R, Wohleb ES, Land BB, DiLeone RJ, et al. Optogenetic stimulation of infralimbic PFC reproduces ketamine's rapid and sustained antidepressant actions. Proc Natl Acad Sci U S A. 2015;112:8106–8111.

58. Hare BD, Shinohara R, Liu RJ, Pothula S, DiLeone RJ, Duman RS. Optogenetic stimulation of medial prefrontal cortex Drd1 neurons produces rapid and long-lasting antidepressant effects. Nat Commun. 2019;10:1–12.

59. Slattery DA, Neumann ID, Cryan JF. Transient inactivation of the infralimbic cortex induces antidepressant-like effects in the rat. J Psychopharmacol. 2011;25:1295–1303.

60. Chen YH, Wu JL, Hu NY, Zhuang JP, Li WP, Zhang SR, et al. Distinct projections from the infralimbic cortex exert opposing effects in modulating anxiety and fear. J Clin Invest. 2021;131.

61. Vidal-Gonzalez I, Vidal-Gonzalez B, Rauch SL, Quirk GJ. Microstimulation reveals opposing influences of prelimbic and infralimbic cortex on the expression of conditioned fear. Learn Mem. 2006;13:728–733.

62. Sierra-Mercado D, Padilla-Coreano N, Quirk GJ. Dissociable roles of prelimbic and infralimbic cortices, ventral hippocampus, and basolateral amygdala in the expression and extinction of conditioned fear. Neuropsychopharmacology. 2011;36:529–538.

63. Arruda-Carvalho M, Clem RL. Prefrontal-amygdala fear networks come into focus. Front Syst Neurosci. 2015;9:145.

64. Arruda-Carvalho M, Clem RL. Pathway-selective adjustment of prefrontal-amygdala transmission during fear encoding. J Neurosci. 2014;34:15601–15609.

65. Quirk GJ, Russo GK, Barron JL, Lebron K. The role of ventromedial prefrontal cortex in the recovery of extinguished fear. J Neurosci. 2000;20:6225–6231.

66. Sotres-Bayon F, Sierra-Mercado D, Pardilla-Delgado E, Quirk GJ. Gating of fear in prelimbic cortex by hippocampal and amygdala inputs. Neuron. 2012;76:804–812.

67. Akhter F, Haque T, Sato F, Kato T, Ohara H, Fujio T, et al. Projections from the dorsal peduncular cortex to the trigeminal subnucleus caudalis (medullary dorsal horn) and other lower brainstem areas in rats. Neuroscience. 2014;266:23–37.

68. Kataoka N, Shima Y, Nakajima K, Nakamura K. A central master driver of psychosocial stress responses in the rat. Science (80- ). 2020;367:1105–1112.

69. Nakamura K, Morrison SF. Central sympathetic network for thermoregulatory responses to psychological stress. Aut Neurosci. 2022;237:102918.

70. Nakamura K, Nakamura Y, Kataoka N. A hypothalamomedullary network for physiological responses to environmental stresses. Nat Rev Neurosci. 2022;23:35–52.

71. Diorio D, Viau V, Meaney MJ. The role of the medial prefrontal cortex (cingulate gyrus) in the regulation of hypothalamic-pituitary-adrenal responses to stress. J Neurosci. 1993;13:3839–3847.

72. Radley JJ, Arias CM, Sawchenko PE. Regional differentiation of the medial prefrontal cortex in regulating adaptive responses to acute emotional stress. J Neurosci. 2006;26:12967–12976.

73. Tavares RF, Correa FM. Role of the medial prefrontal cortex in cardiovascular responses to acute restraint in rats. Neuroscience. 2006;143:231–240.

74. Radley JJ, Gosselink KL, Sawchenko PE. A discrete GABAergic relay mediates medial prefrontal cortical inhibition of the neuroendocrine stress response. J Neurosci. 2009;29:7330–7340.

75. Olff M, Guzelcan Y, de Vries GJ, Assies J, Gersons BP. HPA- and HPT-axis alterations in chronic posttraumatic stress disorder. Psychoneuroendocrinology. 2006;31:1220–1230.

76. Park J, Marvar PJ, Liao P, Kankam ML, Norrholm SD, Downey RM, et al. Baroreflex dysfunction and augmented sympathetic nerve responses during mental stress in veterans with post-traumatic stress disorder. J Physiol. 2017;595:4893–4908.

77. Fonkoue IT, Marvar PJ, Norrholm S, Li Y, Kankam ML, Jones TN, et al. Symptom severity impacts sympathetic dysregulation and inflammation in post-traumatic stress disorder (PTSD). Brain Behav Immun. 2020;83:260–269.

78. Teed AR, Feinstein JS, Puhl M, Lapidus RC, Upshaw V, Kuplicki RT, et al. Association of Generalized Anxiety Disorder With Autonomic Hypersensitivity and Blunted Ventromedial Prefrontal Cortex Activity During Peripheral Adrenergic Stimulation: A Randomized Clinical Trial. JAMA Psychiatry. 2022;79:323–332.

79. Botterill JJ, Khlaifia A, Walters BJ, Brimble MA, Scharfman HE, Arruda-Carvalho M. Off-Target Expression of Cre-Dependent Adeno- Associated Viruses in Wild-Type C57BL/6J Mice. ENeuro. 2021;8:1–16.

80. Arruda-Carvalho M, Wu W, Cummings KA, Clem RL. Optogenetic examination of prefrontal-amygdala synaptic development. J Neurosci. 2017. 2017. https://doi.org/10.1523/JNEUROSCI.3097-16.2017.

81. Seibenhener ML, Wooten MC. Use of the open field maze to measure locomotor and anxiety-like behavior in mice. J Vis Exp. 2015:e52434.

82. Ueno H, Takahashi Y, Suemitsu S, Murakami S, Kitamura N, Wani K, et al. Effects of repetitive gentle handling of male C57BL/6NCrl mice on comparative behavioural test results. Sci Rep. 2020;10:3509.

83. Botterill JJ, Vinod KY, Gerencer KJ, Teixeira CM, LaFrancois JJ, Scharfman HE. Bidirectional regulation of cognitive and anxiety-like behaviors by dentate gyrus mossy cells in male and female mice. J Neurosci. 2021;41:2475–2495.

84. Komada M, Takao K, Miyakawa T. Elevated plus maze for mice. J Vis Exp. 2008. 2008. https://doi.org/10.3791/1088.

85. Steru L, Chermat R, Thierry B, Simon P. The tail suspension test: a new method for screening antidepressants in mice. Psychopharmacol. 1985;85:367–370.

86. Ueno H, Takahashi Y, Murakami S, Wani K, Matsumoto Y, Okamoto M, et al. Effect of simultaneous testing of two mice in the tail suspension test and forced swim test. Sci Rep. 2022;12:9224.

87. Nandi A, Virmani G, Barve A, Marathe S. DBscorer: An open-source software for automated accurate analysis of rodent behavior in forced swim test and tail suspension test. ENeuro. 2021;8.

88. Arruda-Carvalho M, Sakaguchi M, Akers KG, Josselyn S a, Frankland PW. Posttraining ablation of adult-generated neurons degrades previously acquired memories. J Neurosci. 2011;31:15113–15127.

89. Porsolt RD, Bertin A, Jalfre M. Behavioral despair in mice: a primary screening test for antidepressants. Arch Int Pharmacodyn Ther. 1977;229:327–336.

90. Can A, Dao DT, Arad M, Terrillion CE, Piantadosi SC, Gould TD. The mouse forced swim test. J Vis Exp. 2012:e3638.

91. Kara NZ, Stukalin Y, Einat H. Revisiting the validity of the mouse forced swim test: Systematic review and meta-analysis of the effects of prototypic antidepressants. Neurosci Biobehav Rev. 2018;84:1–11.

92. Can A, Dao DT, Arad M, Terrillion CE, Piantadosi SC, Gould TD. The mouse forced swim test. J Vis Exp. 2011:1–6.

93. Samifanni R, Zhao M, Cruz-Sanchez A, Satheesh A, Mumtaz U, Arruda-Carvalho M. Developmental emergence of persistent memory for contextual and auditory fear in mice. Learn

Mem. 2021;28:414–421.

94. Thompson KJ, Khajehali E, Bradley SJ, Navarrete JS, Huang XP, Slocum S, et al. DREADD Agonist 21 Is an Effective Agonist for Muscarinic-Based DREADDs in Vitro and in Vivo. ACS Pharmacol Transl Sci. 2018;1:61–72.

95. Sullivan RM, Gratton A. Prefrontal cortical regulation of hypothalamic-pituitary-adrenal function in the rat and implications for psychopathology: side matters. Psychoneuroendocrinology. 2002;27:99–114.

96. Jaferi A, Bhatnagar S. Corticotropin-releasing hormone receptors in the medial prefrontal cortex regulate hypothalamic-pituitary-adrenal activity and anxiety-related behavior regardless of prior stress experience. Brain Res. 2007;1186:212–223.

97. Weinberg MS, Johnson DC, Bhatt AP, Spencer RL. Medial prefrontal cortex activity can disrupt the expression of stress response habituation. Neuroscience. 2010;168:744–756.

98. Haberly LB, Price JL. Association and commissural fiber systems of the olfactory cortex of the rat II. Systems originating in the olfactory peduncle. J Comp Neurol. 1978;181:781–807.

99. Franklin KBJ, Paxinos G. The Mouse Brain in Stereotaxic Coordinates (map). 2007.

100. Paxinos G, Watson C. The rat brain in stereotaxic coordinates. 1997.

101. Hurley KM, Herbert H, Moga MM, Saper CB. Efferent projections of the infralimbic cortex of the rat. J Comp Neurol. 1991;308:249–276.

102. Fisk GD, Wyss JM. Descending projections of infralimbic cortex that mediate stimulation-evoked changes in arterial pressure. Brain Res. 2000;859:83–95.

103. Ferguson BR, Gao WJ. Thalamic Control of Cognition and Social Behavior Via Regulation of Gamma-Aminobutyric Acidergic Signaling and Excitation/Inhibition Balance in the Medial Prefrontal Cortex. Biol Psychiatry. 2018;83:657–669.

104. Ouhaz Z, Ba-M'hamed S, Mitchell AS, Elidrissi A, Bennis M. Behavioral and cognitive changes after early postnatal lesions of the rat mediodorsal thalamus. Behav Brain Res. 2015;292:219–232.

105. Ouhaz Z, Ba-M'hamed S, Bennis M. Morphological, structural, and functional alterations of the prefrontal cortex and the basolateral amygdala after early lesion of the rat mediodorsal thalamus. Brain Struct Funct. 2017;222:2527–2545.

106. Beracochea D, Krazem A. Effects of mammillary body and mediodorsal thalamic lesions on elevated plus maze exploration. Neuroreport. 1991;2:793–796.

107. Li Y, Li S, Wei C, Wang H, Sui N, Kirouac GJ. Orexins in the paraventricular nucleus of the thalamus mediate anxiety-like responses in rats. Psychopharmacology (Berl). 2010;212:251–265.

108. Kirouac GJ. Placing the paraventricular nucleus of the thalamus within the brain circuits that control behavior. Neurosci Biobehav Rev. 2015;56:315–329.

109. Kooiker CL, Birnie MT, Baram TZ. The Paraventricular Thalamus: A Potential Sensor and Integrator of Emotionally Salient Early-Life Experiences. Front Behav Neurosci. 2021;15:1–9.

110. Barson JR, Leibowitz SF. GABA-induced inactivation of dorsal midline thalamic subregions has distinct effects on emotional behaviors. Neurosci Lett. 2015;609:92–96.

111. Zhao D, Wang D, Wang W, Dai J, Cui M, Wu M, et al. The altered sensitivity of acute stress induced anxiety-related behaviors by modulating insular cortex-paraventricular thalamus-bed nucleus of the stria terminalis neural circuit. Neurobiol Dis. 2022;174:105890.

112. Shin LM, Liberzon I. The neurocircuitry of fear, stress, and anxiety disorders. Neuropsychopharmacology. 2010;35:169–191.

113. Shi T, Feng S, Wei M, Zhou W. Role of the anterior agranular insular cortex in the modulation of fear and anxiety. Brain Res Bull. 2020;155:174–183.

114. Shi TY, Feng SF, Wei MX, Huang Y, Liu G, Wu HT, et al. Kainate receptor mediated presynaptic LTP in agranular insular cortex contributes to fear and anxiety in mice. Neuropharmacology. 2018;128:388–400.

115. Li H, Chen L, Li P, Wang X, Zhai H. Insular muscarinic signaling regulates anxiety-like behaviors in rats on the elevated plus-maze. Behav Brain Res. 2014;270:256–260.

116. Méndez-Ruette M, Linsambarth S, Moraga-Amaro R, Quintana-Donoso D, Méndez L, Tamburini G, et al. The role of the rodent insula in anxiety. Front Physiol. 2019;10:1–10.

117. Linley SB, Athanason AC, Rojas AKP, Vertes RP. Role of the reuniens and rhomboid thalamic nuclei in anxiety-like avoidance behavior in the rat. Hippocampus. 2021;31:756–769.

118. Felix-Ortiz AC, Tye KM. Amygdala inputs to the ventral hippocampus bidirectionally modulate social behavior. J Neurosci. 2014;34:586–595.

119. Felix-Ortiz AC, Beyeler A, Seo C, Leppla CA, Wildes CP, Tye KM. BLA to vHPC Inputs Modulate Anxiety-Related Behaviors. Neuron. 2013;79:658–664.

120. Tye KM, Prakash R, Kim S-Y, Fenno LE, Grosenick L, Zarabi H, et al. Amygdala circuitry mediating reversible and bidirectional control of anxiety. Nature. 2011;471:358–362.

121. Adhikari A, Lerner TN, Finkelstein J, Pak S, Jennings JH, Davidson TJ, et al. Basomedial amygdala mediates top-down control of anxiety and fear. Nature. 2015;527:179–185.

122. Daviu N, Bruchas MR, Moghaddam B, Sandi C, Beyeler A. Neurobiological links between stress and anxiety. Neurobiol Stress. 2019;11:100191.

123. Wang GQ, Cen C, Li C, Cao S, Wang N, Zhou Z, et al. Deactivation of excitatory neurons in the prelimbic cortex via Cdk5 promotes pain sensation and anxiety. Nat Commun. 2015;6.

124. Feldman S, Conforti N. Modifications of adrenocortical responses following frontal cortex simulation in rats with hypothalamic deafferentations and medial forebrain bundle lesions. Neuroscience. 1985;15:1045–1047.

125. Figueiredo HF, Bruestle A, Bodie B, Dolgas CM, Herman JP. The medial prefrontal cortex differentially regulates stress-induced c-fos expression in the forebrain depending on type of stressor. Eur J Neurosci. 2003;18:2357–2364.

126. Van Eden CG, Buijs RM. Functional neuroanatomy of the prefrontal cortex: Autonomic interactions. Prog Brain Res. 2000;126:49–62.

127. Brake WG, Flores G, Francis D, Meaney MJ, Srivastava LK, Gratton A. Enhanced nucleus accumbens dopamine and plasma corticosterone stress responses in adult rats with neonatal excitotoxic lesions to the medial prefrontal cortex. Neuroscience. 2000;96:687–695.

128. Crane JW, Ebner K, Day TA. Medial prefrontal cortex suppression of the hypothalamic-pituitary-adrenal axis response to a physical stressor, systemic delivery of interleukin-1β. Eur J Neurosci. 2003;17:1473–1481.

129. Sullivan RM, Gratton A. Lateralized effects of medial prefrontal cortex lesions on neuroendocrine and autonomic stress responses in rats. J Neurosci. 1999;19:2834–2840.

130. Buijs RM, Van Eden CG. The integration of stress by the hypothalamus, amygdala and prefrontal cortex: Balance between the autonomic nervous system and the neuroendocrine system. Prog

Brain Res. 2000;126:117–132.

131. Choi DC, Furay AR, Evanson NK, Ulrich-Lai YM, Nguyen MMN, Ostrander MM, et al. The role of the posterior medial bed nucleus of the stria terminalis in modulating hypothalamic-pituitary-adrenocortical axis responsiveness to acute and chronic stress. Psychoneuroendocrinology. 2008;33:659–669.

132. Spencer SJ, Buller KM, Day TA. Medial prefrontal cortex control of the paraventricular hypothalamic nucleus response to psychological stress: Possible role of the bed nucleus of the stria terminalis. J Comp Neurol. 2005;481:363–376.

133. Pizzagalli DA, Roberts AC. Prefrontal cortex and depression. Neuropsychopharmacology. 2022;47:225–246.

134. Challis C, Beck SG, Berton O. Optogenetic modulation of descending prefrontocortical inputs to the dorsal raphe bidirectionally bias socioaffective choices after social defeat. Front Behav Neurosci. 2014;8:1–14.

135. Miller OH, Bruns A, Ben Ammar I, Mueggler T, Hall BJ. Synaptic Regulation of a Thalamocortical Circuit Controls Depression-Related Behavior. Cell Rep. 2017;20:1867–1880.

136. Hamani C, MacHado DC, Hipólide DC, Dubiela FP, Suchecki D, MacEdo CE, et al. Deep brain stimulation reverses anhedonic-like behavior in a chronic model of depression: Role of serotonin and brain derived neurotrophic factor. Biol Psychiatry. 2012;71:30–35.

137. Kumar S, Black SJ, Hultman R, Szabo ST, DeMaio KD, Du J, et al. Cortical control of affective networks. J Neurosci. 2013;33:1116–1129.

138. Vialou V, Bagot RC, Cahill ME, Ferguson D, Robison AJ, Dietz DM, et al. Prefrontal Cortical Circuit for Depression- and Anxiety- Related Behaviors Mediated by Cholecystokinin : Role of □ FosB. J Neurosci. 2014;34:3878–3887.

139. Bagot RC, Parise EM, Peña CJ, Zhang H-X, Maze I, Chaudhury D, et al. Ventral hippocampal afferents to the nucleus accumbens regulate susceptibility to depression. Nat Commun. 2015;6:7062.

140. Covington HE, Lobo MK, Maze I, Vialou V, Hyman JM, Zaman S, et al. Antidepressant effect of optogenetic stimulation of the medial prefrontal cortex. J Neurosci. 2010;30:16082–16090.

141. Perova Z, Delevich K, Li B. Depression of excitatory synapses onto parvalbumin interneurons in the medial prefrontal cortex in susceptibility to stress. J Neurosci. 2015;35:3201–3206.

142. Warden MR, Selimbeyoglu A, Mirzabekov JJ, Lo M, Thompson KR, Kim SY, et al. A prefrontal cortex-brainstem neuronal projection that controls response to behavioural challenge. Nature. 2012;492:428–432.

143. Muir J, Lopez J, Bagot RC. Wiring the depressed brain: optogenetic and chemogenetic circuit interrogation in animal models of depression. Neuropsychopharmacology. 2019;44:1013–1026.

144. Do-Monte FH, Manzano-Nieves G, Quiñones-Laracuente XK, Ramos-Medina L, Quirk GJ. Revisiting the Role of Infralimbic Cortex in Fear Extinction with Optogenetics. J Neurosci. 2015;35:3607–3615.

145. Bukalo O, Pinard CR, Silverstein S, Brehm C, Hartley ND, Whittle N, et al. Prefrontal inputs to the amygdala instruct fear extinction memory formation. Sci Adv. 2015;1:e1500251–e1500251.

146. Cho J-H, Deisseroth K, Bolshakov VY. Synaptic encoding of fear extinction in mPFC-amygdala circuits. Neuron. 2013;80:1491–1507.

147. Arruda-carvalho M, Clem RL. Prefrontal-amygdala fear networks come into focus. 2015;9:1–5.

148. Milad MR, Wright CI, Orr SP, Pitman RK, Quirk GJ, Rauch SL. Recall of fear extinction in humans activates the ventromedial prefrontal cortex and hippocampus in concert. Biol Psychiatry. 2007;62:446–454.

149. du Plessis KC, Basu S, Rumbell TH, Lucas EK. Sex-Specific Neural Networks of Cued Threat Conditioning: A Pilot Study. Front Syst Neurosci. 2022;16:1–11.

150. McLean CP, Asnaani A, Litz BT, Hofmann SG. Gender differences in anxiety disorders: Prevalence, course of illness, comorbidity and burden of illness. J Psychiatr Res. 2011;45:1027–1035.

151. Kessler RC, Sonnega A, Nelson CB, Bromet E. Posttraumatic Stress Disorder in the National Comorbidity Survey. Arch Gen Psychiatry. 1995;52.

152. Bangasser DA, Cuarenta A. Sex differences in anxiety and depression: circuits and mechanisms. Nat Rev Neurosci. 2021;22:674–684.

153. Dart AM, Du XJ, Kingwell BA. Gender, sex hormones and autonomic nervous control of the cardiovascular system. Cardiovasc Res. 2002;53:678–687.

154. Hinojosa-Laborde C, Chapa I, Lange D, Haywood J. Gender differences in sympathetic nervous system regulation. Clin Exp Pharmacol Physiol. 1999;26:122–126.

155. Barsha G, Denton KM, Mirabito Colafella KM. Sex- and age-related differences in arterial pressure and albuminuria in mice. Biol Sex Differ. 2016;7:1–15.

156. Colafella KMM, Denton KM. Sex-specific differences in hypertension and associated cardiovascular disease. Nat Rev Nephrol. 2018;14:185–201.

157. Fuchs T, Jefferson SJ, Hooper A, Yee PH, Maguire J, Luscher B. Disinhibition of somatostatin-positive GABAergic interneurons results in an anxiolytic and antidepressant-like brain state. Mol Psychiatry. 2017;22:920–930.

158. Cummings KA, Clem RL. Prefrontal somatostatin interneurons encode fear memory. Nat Neurosci. 2020;23:61–74.

159. Xu H, Liu L, Tian Y, Wang J, Li J, Zheng J, et al. A Disinhibitory Microcircuit Mediates Conditioned Social Fear in the Prefrontal Cortex. Neuron. 2019;102:668-682 e5.

160. Cummings KA, Bayshtok S, Dong TN, Kenny PJ, Clem RL. Control of fear by discrete prefrontal GABAergic populations encoding valence-specific information. Neuron. 2022;110:3036-3052 e5.

161. Page CE, Shepard R, Heslin K, Coutellier L. Prefrontal parvalbumin cells are sensitive to stress and mediate anxiety-related behaviors in female mice. Sci Rep. 2019;9:1–9.

162. Todorović N, Mićić B, Schwirtlich M, Stevanović M, Filipović D. Subregion-specific Protective Effects of Fluoxetine and Clozapine on Parvalbumin Expression in Medial Prefrontal Cortex of Chronically Isolated Rats. Neuroscience. 2019;396:24–35.